Eindhoven University of Technology

MASTER

Moisture-induced buckling of paper sheets

de Böck, R.

Award date:
2015

Link to publication

Disclaimer
This document contains a student thesis (bachelor's or master's), as authored by a student at Eindhoven University of Technology. Student theses are made available in the TU/e repository upon obtaining the required degree. The grade received is not published on the document as presented in the repository. The required complexity or quality of research of student theses may vary by program, and the required minimum study period may vary in duration.

General rights
Copyright and moral rights for the publications made accessible in the public portal are retained by the authors and/or other copyright owners and it is a condition of accessing publications that users recognise and abide by the legal requirements associated with these rights.

- Users may download and print one copy of any publication from the public portal for the purpose of private study or research.
- You may not further distribute the material or use it for any profit-making activity or commercial gain

Moisture-induced buckling of paper sheets

Rien de Böck

Under supervision of:

Eindhoven University of Technology
Prof. dr. ir. B. (Barry) Koren
Dr. ir. J.M.L. (Jos) Maubach
Dr. ir. A.A.F. (Fons) van de Ven

Océ
Dr. ir. L.H. (Louis) Saes

A thesis submitted to Eindhoven University of Technology in partial fulfillment of the requirements for the degree of
Master of Science
Venlo, 14 December 2015

Abstract

The effect of a change in moisture content on the geometry of a sheet of paper is investigated with two approaches. A theoretical model based on geometrically nonlinear elasticity theory is formulated and analytical results are presented for two reference problems: a circular plate wetted in the center, and a rectangular plate wetted at the edges. The circular case is solved directly, for the rectangular case variational methods are used. Furthermore, commercially available finite element software is used to simulate the plates. This numerical method is compared to the analytical method for both reference problems and the influence of parameters affecting the change in geometry is investigated.

Acknowledgements

Before getting into the mathematical formulations and scientific considerations, I would like to take a minute to thank everyone who in some way or another helped me in making this thesis possible.

For this project I have had the pleasure of working under supervision of Louis Saes at Océ. The freedom he gave me in choosing a direction for the project, while gently steering me in the direction of research that was actually practical, was exactly what I needed to focus my thoughts. I particularly enjoyed the dialogues about the various aspects of modeling, which often devolved into philosophical discussions. I thank him for the opportunity he gave me to work on this project and for all he has done since.

I was blessed to receive excellent guidance from Eindhoven university of technology by Barry Koren, Jos Maubach and Fons van de Ven. The discussions we had at the university and at Océ always offered me new viewpoints and inspiration on how to proceed. In particular I owe Fons my gratitude for the tireless work he put into commenting on my intermediate work and sharing parts of his vast knowledge of mechanics.

This thesis was a result of working at Océ in Venlo for nine months. I felt at home in the environment created by everyone at the department, where serious work was alternated with discussions about physics, politics and leisure time, while enjoying some vlaai.

During the project I have had productive discussions with Ron Peerlings and Piet Schreurs from the mechanical engineering department. Their expertise on the modeling and simulation of mechanics was greatly appreciated. For advice on the specifics of how to implement the simulation and the selection of the right options from the huge arsenal the software provides I thank Maarten Oudendijk of In Summa.

All work and no play would have made me a dull boy. During the time I have been studying in Eindhoven I was involved in many events, giving me fond memories and invaluable life experience. I feel extremely fortunate with the friends I made inside and outside of GEWIS, with all of the games of foosball, playing cards and borrels. In particular, the 31st board of GEWIS, my fellow university council members of Groep-één, as well as the members of committees in which I was glad to take part.

Last but certainly not least I am grateful to my family, for the support they gave me, morally and otherwise, and for always encouraging me and believing in me.

This page is intentionally left in its initial, undeformed, configuration.

Contents

Chapter 1

Introduction

1.1 Motivation for this research

In the process of making ever-faster industrially used sheet-fed printers, Océ has recently released the *Varioprint i300*. This colossal machine, shown in Figure 1.1, can print up to 17500 A4 images per hour on various types of paper [1]. It incorporates the inkjet printing technique in a way that a sheet surface passes

Figure 1.1: The Varioprint i300 unit

underneath the ink nozzles only once. This means that at full speed 80 million droplets of ink per second have to be dropped on the paper sheets. Great precision is required here; a deviation of only 0.01 mm, a tenth of the thickness of a paper sheet, is visible to the naked eye and should be avoided. This ambitious technical demand makes it desirable to align the ink nozzles as closely as possible to the sheet surface. However, paper sheets are not entirely flat. To design the printer such that it is capable of handling paper sheets with thickness variations, research into paper deformations is required. This thesis focuses on the deformations caused by moisture absorption. The goal is to gain insight in the underlying physical process and the influence of the relevant parameters.

1.2 Paper as an engineering material

Paper as we know it today is a widely used material due to its desirable properties for writing and printing. Unfortunately, from an engineering standpoint, paper is an impracticable material, [2], [3]. Its physical

properties are difficult to model, because of its complex micro-scale structure. Paper mainly consists of a network of slender wood fibres with a length and width in the range of 1-3 mm and 20-40 μm, respectively. Since paper is only approximately 0.1 mm thick, the network is planar and almost two-dimensional. The physical properties of paper depend on the in-plane direction chosen. In order to get a better understanding of this property, known as anisotropy, we briefly consider the manufacturing process.

The first step is to cut wood into chips and then to disintegrate it into so-called pulp. This leaves slender pulp fibres. Next the pulp is bleached and it undergoes a process called beating, which causes the fibres to become more flexible so they can eventually bond better to form a tight web.

A mixture of about 99% water and 1% pulp enters the paper machine on a conveyor belt. This causes the pulp to mix uniformly, which results in increased homogeneity of the end product. In the paper machine the water is extracted from the mix in multiple ways and at the end of the machine a roll of paper comes out.

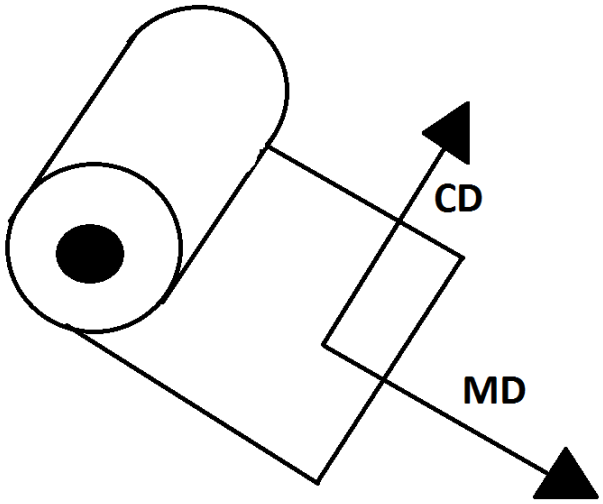

Figure 1.2: Machine direction (MD) and cross direction (CD) on a roll of paper

Despite the efforts to create a roll of paper to be as homogeneous as possible, the effects of heterogeneity on the end product cannot be neglected. Also, speed differences in the paper machine cause the fibres to be oriented more in the longitudinal direction of the roll than in the other directions. This is the direction in which the paper travels through the machine and is therefore referred to as *machine direction* (MD). The perpendicular direction is referred to as *cross direction* (CD), as shown in Figure 1.2. This fibre orientation causes differences in physical properties of paper between CD and MD. One of the differences of great importance to this research is the swelling of paper fibres when absorbing water. The fibres swell more in width than in length by a factor of 20, which at macro-scale results in a difference with a factor of 5.

1.3 Moisture content

To research the water-induced deformations of paper we need some measure of the amount of water contained in the sheet. The *moisture content* (MC) serves this purpose. It is defined as the mass percentage of the paper that originates from the water it contains.

When the source of the water in the sheet is moisture exchange with the air, the *relative humidity* (RH) is an important quantity. It is defined as the amount of water vapor the air contains, as a percentage of what it could maximally contain. When paper is transported to an area with new environmental circumstances it will adapt to the new humidity until it reaches an equilibrium. The relationship between the RH and the

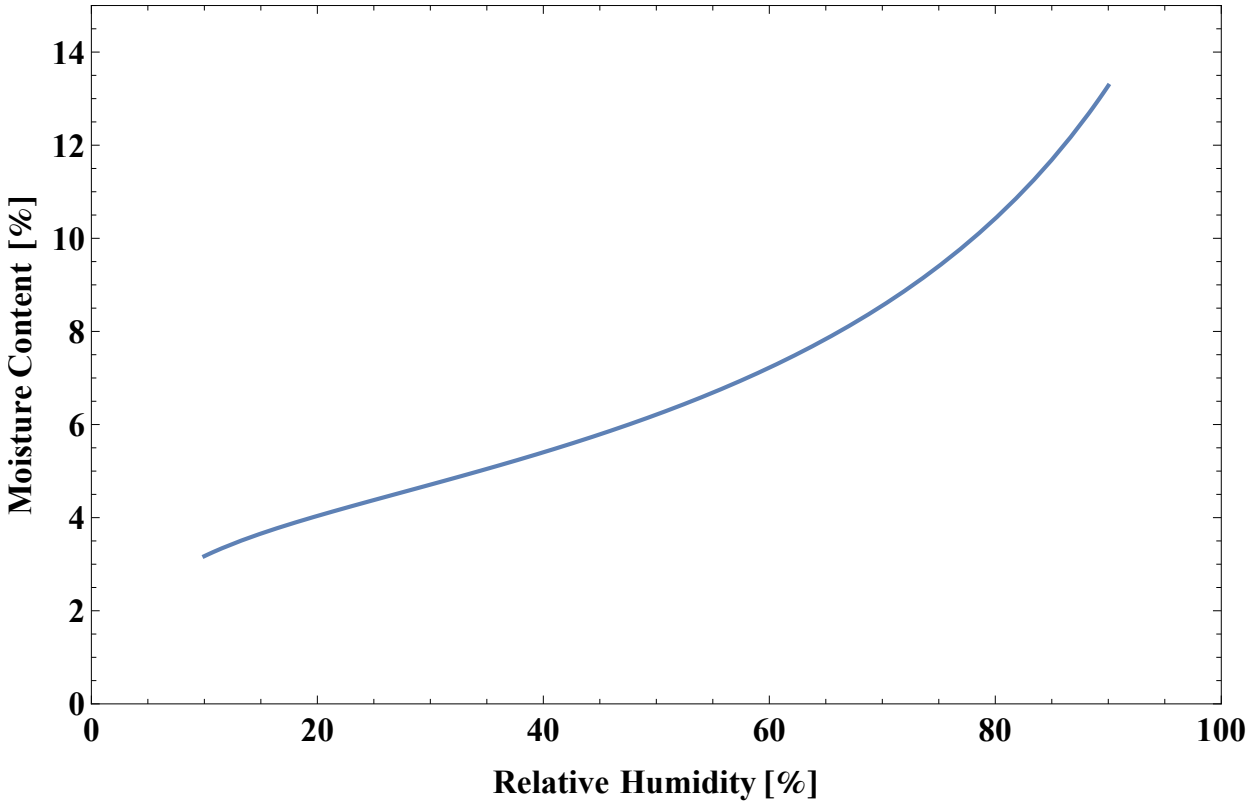

Figure 1.3: The sorption isotherm of a typical paper sheet.

corresponding equilibrium value of MC is given by a *sorption isotherm*. This has been researched by Océ in the past [4], a characteristic example of such a sorption isotherm is given in Figure 1.3. As we can see, the change in moisture content caused by absorption from the air could be up to 10 %.

1.4 Solution approach

To research out-of-plane deformations of paper, we consider a homogeneous single sheet of paper initially in equilibrium with its environment, exposed to an increase of moisture content in a certain region of the sheet. There are three ways to conduct research on such a physical situation: experimentation, theoretical analysis and numerical simulation. Experimentation has proven to be complicated and time-consuming, environmental conditions need to be controlled and the dynamic measurement of the shape of a paper sheet is complicated. Considering the amount of possible influential parameters many experiments have to be executed and due to the heterogeneity of paper, it is difficult to distinguish between effects due to parameters and those due to randomness. Therefore this report will focus on the latter two methods. For the theoretical research the paper is modeled as an orthotropic elastic medium. For the numerical solution method the commercially available software packages Marc/Mentat [14] and MATLAB [15] will be used; Matlab for the pre- and postprocessing and Marc/Mentat for the finite element calculations.

We will consider two reference problems; an isotropic circular plate, wetted at the center and a rectangular orthotropic plate, exposed to a rise in moisture content along the edges. Much emphasis will be on comparing the results obtained from the theory and from the simulation with regard to the solution of these reference problems.

1.5 The phenomenon of buckling

When holding a piece of paper at opposite ends and moving the ends together, we see that the paper deforms out of its flat position, even though virtually no force is applied in this direction. This behavior is caused by a phenomenon called *buckling*, an instability of the initial flat position due to compressing forces. When partially wetting a paper sheet, the constrained growth of the fibres in the wet part of the sheet induces compressing forces resulting in buckling as well.

Mathematically, the initial flat position is stable up until a certain threshold of forces is reached, after which buckling occurs, resulting in out-of-plane deformations with the order of magnitude of the thickness of the sheet. Since the initial position is not perfectly flat and the paper is not homogeneous the unstable position cannot be maintained after the buckling threshold is reached.

Determining the shape after deformation of a paper sheet under the influence of external factors essentially comes down to a minimization problem. Once the potential energy due to bending out-of-plane exceeds the potential energy due to stretching, buckling occurs and the paper takes the shape that minimizes the total potential energy.

In the remainder of this report, much emphasis is on describing the behavior of the sheet up to and including the onset of buckling. We use the knowledge gained about the pre-buckling situation to compare the results obtained by the theory and the simulation; the displacement, the stresses, the buckling threshold and the deflection shape.

1.6 Outline of the report

In Chapter 2 the theory to model large out-of-plane deformations resulting from moisture-induced stresses is developed, based on geometrically nonlinear elasticity. This theory is used to model two reference problems. Chapter 3 describes a circular plate wetted at its center and the analytical method used to tackle it and Chapter 4 does the same for a rectangular orthotropic plate. The numerical simulation is explained in Chapter 5. The two methods are compared in Chapter 6 for both reference problems and the influence of the relevant parameters is explored. Chapter 7 lists the results found and links them to the practical situations encountered in practice.

1.7 Deliverables

Besides the research presented in this report, some software used to model the paper has been delivered. An input file for Marc/Mentat [14] to model the circular plate is composed and a MATLAB [15] file has been written to produce such files. A Mathematica [16] file used for the analytical method for the circular plate as described in Chapter 3 has been written. An existing MATLAB code made at Océ, used to create input files for Marc/Mentat for rectangular plates has been improved to produce robust simulations, resulting in solutions agreeing with those of the analytical method. Finally, a Mathematica file has been written to perform the variational method on a rectangular plate, as described in Chapter 4.

1.8 Results and discussion

The geometrically nonlinear elasticity model derived in this report proved to be solvable directly for the circular plate. The pre-buckling stress, the buckling threshold and the shape of the plate immediately after buckling were found in terms of Bessel functions. These results agree well with the simulated results for various values of the relevant parameters.

The influence of the parameters on the value of the buckling threshold was researched. The sheet's Young's modulus has no effect on the buckling threshold, since the bending and stretching energy both depend linearly on it. Poisson's ratio barely influences the buckling threshold, leading to the conclusion that

the buckling threshold is almost completely defined by the geometry of the plate and the wetted region. The buckling threshold depends quadratically on the thickness: thinner plates require lower stress levels to buckle. The buckling threshold is high when the wetted area is either a very large or a very small part of the plate, and lower for intermediate values.

The reference problem of the rectangular plate is solved using variational methods. The pre-buckling stress was found and the buckling threshold was approximated using the Rayleigh-Ritz method for four plates with various properties. The results agree well with the simulation.

This page is intentionally left in its initial, undeformed, configuration.

Chapter 2

Derivation of the mathematical model

In this chapter the mathematical model we use to describe the stresses by wetting of paper and the buckling resulting from it will be built up in steps. First we will introduce the concept of linear elasticity and its mathematical formulations. Then linear thin plate theory, *Kirchhoff theory*, will be introduced to reduce the model to a two-dimensional situation under the assumption that the sheet is thin and that out-of-plane deformations are small. Also, the model is extended to include stresses that result from wetting. As it turns out, after buckling this linear theory is not sufficient to describe the large out-of-plane deformations that occur, therefore the model is extended and *von Kármán theory* will be introduced to obtain equations coupling bending and stretching.

2.1 Kinematics, stresses and elasticity theory

2.1.1 Elasticity

The concept of elasticity refers to a material property in which a solid that deforms due to external influences, returns to its initial, undeformed, configuration when it is no longer exposed to these external influences [6]. In the case of wetting of paper, elasticity is a valid assumption as long as no effects due to repeated wetting and drying, hysteresis effects, are considered [3]. In this report a one-time wetting will be considered and therefore we will model paper as a perfectly elastic material. We will assume that the material is homogeneous and model it as a continuum, such that a small element of sheet exhibits the same physical properties as the entire sheet.

2.1.2 Configuration and deformations

We consider a body as a set of material points, $\mathcal{P} \in \mathcal{B}$, and call its reference configuration $\mathcal{G}_R \in \mathbb{R}^3$.

The configuration $\mathcal{G}_R$ is the region of $\mathbb{R}^3$ the body occupies in its initial state. We denote positions in this region by $\boldsymbol{X} \in \mathcal{G}_R, \boldsymbol{X} = \{X_\alpha, \alpha = 1, 2, 3\}$; this represents the undeformed body.
Likewise, we define for the body $\mathcal{B}$ a configuration $\mathcal{G} \in \mathbb{R}^3$ and denote positions in this body by $\boldsymbol{x} \in \mathcal{G}, \boldsymbol{x} = \{x_i, i = 1, 2, 3\}$, to represent the deformed body. We assume the body to be continuous, which, according to the *localization theorem* means we can assign a nonzero value for the density to each point. The two coordinate systems are known as Lagrangian and Eulerian, respectively [6].
We assume that a bijection exists between the two coordinate systems, indicating that no cracks or holes form in the body due to the deformation. We denote this bijection by:

$$\boldsymbol{x} = \boldsymbol{\varphi}(\boldsymbol{X}), \quad \boldsymbol{X} = \boldsymbol{\Psi}(\boldsymbol{x}). \tag{2.1}$$

The displacement of a point can be expressed in both coordinate systems and is defined as $\boldsymbol{u} := \boldsymbol{x} - \boldsymbol{X}, \tilde{\boldsymbol{u}} :=$

$\boldsymbol{\varphi}(\boldsymbol{X}) - \boldsymbol{X}, \overline{\boldsymbol{u}} := \boldsymbol{x} - \boldsymbol{\Psi}(\boldsymbol{x})$. We define the *deformation gradient* by

$$\mathcal{F} := \frac{\partial \boldsymbol{x}}{\partial \boldsymbol{X}} = \mathcal{I} + \frac{\partial \tilde{\boldsymbol{u}}}{\partial \boldsymbol{X}}, \tag{2.2}$$

where $\mathcal{I}$ is the identity tensor of suitable dimensions. The components of $\mathcal{F}$ are $F_{i\alpha} := \partial x_i / \partial X_\alpha = x_{i,\alpha} = \delta_{i\alpha} + u_{i,\alpha}$, using the comma to denote differentiation, and the notational difference between Greek and Latin letters to distinguish between the coordinate systems, while δ_{ij} denotes the Kronecker delta.
As a measure for the changes in shape of the body (called *pure deformations*) we introduce the *Cauchy deformation tensor*, also called strain tensor, by $\mathcal{E} := \frac{1}{2}(\mathcal{F}^T\mathcal{F} - \mathcal{I})$, or component-wise $\varepsilon_{\alpha\beta} = \frac{1}{2}(F_{i\alpha}F_{i\beta} - \delta_{\alpha\beta})$, where we use the Einstein summation convention. The choice for the Cauchy deformation tensor is made because this deformation tensor is equal to zero if and only if no deformations occur and because it is rotation-invariant. Using the definition of $\mathcal{F}$, we find

$$\varepsilon_{\alpha\beta} = \frac{1}{2}\Big(u_{\beta,\alpha} + u_{\alpha,\beta} + \frac{1}{2}u_{k,\alpha}u_{k,\beta}\Big). \tag{2.3}$$

This is valid in both coordinate systems. We note that this deformation tensor is symmetric by definition and nonlinear in $\nabla \boldsymbol{u}$. Many applications of elasticity theory involve small deformations, which justifies use of linear theory. In the following we assume that $|\nabla \boldsymbol{u}| \ll 1$ and that no rigid-body motions occur. As a consequence of these assumptions we approximate

$$\frac{\partial \boldsymbol{u}}{\partial \boldsymbol{X}} = \frac{\partial \boldsymbol{u}}{\partial \boldsymbol{x}}\frac{\partial \boldsymbol{x}}{\partial \boldsymbol{X}} = \frac{\partial \boldsymbol{u}}{\partial \boldsymbol{x}}\left(\mathcal{I} + \frac{\partial \boldsymbol{u}}{\partial \boldsymbol{X}}\right) \doteq \frac{\partial \boldsymbol{u}}{\partial \boldsymbol{x}}, \tag{2.4}$$

where $\doteq$ denotes a linearization. We conclude that under this assumption of linearity we no longer need to distinguish between the two coordinate systems and therefore we will use the notation (x, y, z) for both sets of coordinates.

2.1.3 Compatibility equations

Suppose we now know the deformation tensor and want to determine the displacement field, then we have with (2.3) 6 equation for 3 unknowns $\{u_1, u_2, u_3\}$. Hence, the deformation tensor must obey certain conditions to produce a valid displacement field. These conditions are known as *Saint-Venant equations of compatibility* and they can be written as [5], p. 28:

$$\frac{\partial^2 \varepsilon_{ij}}{\partial x_k \partial x_l} + \frac{\partial^2 \varepsilon_{kl}}{\partial x_i \partial x_j} - \frac{\partial^2 \varepsilon_{ik}}{\partial x_j \partial x_l} - \frac{\partial^2 \varepsilon_{jl}}{\partial x_i \partial x_k} = 0. \tag{2.5}$$

Substitution of the strain tensor (2.3) into this equation shows that it indeed holds for $i, j, k, l = 1, 2, 3$. Including all combinations of values for i, j, k, l would result in $3^4 = 81$ equations. When considering that some are identically satisfied and taking into account that some are duplicates because of symmetry in the

indices, six remain (taking $(x, y, z) = (x_1, x_2, x_3)$):

$$\begin{aligned}
\frac{\partial^2 \varepsilon_{xx}}{\partial y \partial z} &= \frac{\partial}{\partial x}\Big(- \frac{\partial \varepsilon_{yz}}{\partial x} + \frac{\partial \varepsilon_{xz}}{\partial y} + \frac{\partial \varepsilon_{xy}}{\partial z}\Big), \\
\frac{\partial^2 \varepsilon_{yy}}{\partial x \partial z} &= \frac{\partial}{\partial y}\Big(\frac{\partial \varepsilon_{yz}}{\partial x} - \frac{\partial \varepsilon_{xz}}{\partial y} + \frac{\partial \varepsilon_{xy}}{\partial z}\Big), \\
\frac{\partial^2 \varepsilon_{zz}}{\partial x \partial y} &= \frac{\partial}{\partial z}\Big(\frac{\partial \varepsilon_{yz}}{\partial x} + \frac{\partial \varepsilon_{xz}}{\partial y} - \frac{\partial \varepsilon_{xy}}{\partial z}\Big), \\
2\frac{\partial^2 \varepsilon_{xy}}{\partial x \partial y} &= \frac{\partial^2 \varepsilon_{xx}}{\partial y^2} + \frac{\partial^2 \varepsilon_{yy}}{\partial x^2}, \\
2\frac{\partial^2 \varepsilon_{xz}}{\partial x \partial z} &= \frac{\partial^2 \varepsilon_{xx}}{\partial z^2} + \frac{\partial^2 \varepsilon_{zz}}{\partial x^2}, \\
2\frac{\partial^2 \varepsilon_{yz}}{\partial y \partial z} &= \frac{\partial^2 \varepsilon_{yy}}{\partial z^2} + \frac{\partial^2 \varepsilon_{zz}}{\partial y^2}.
\end{aligned} \tag{2.6}$$

2.1.4 Stress

In an elastic material the internal forces acting between parts of the material are of importance to determine the behavior of the material in response to external factors. Considering two adjacent volume elements of the material, the internal force per unit area of contact between the elements is quantified by the stress vector. Let this stress vector $\boldsymbol{t}$ act on an area element with normal $\boldsymbol{n}$ then we can write

$$\boldsymbol{t} = \mathcal{T}\boldsymbol{n}, \tag{2.7}$$

where $\mathcal{T}$, with components σ_{ij}, is called the *stress tensor*. The relation (2.7) is a direct consequence of the conservation of momentum; see for instance [5], p. 35. For materials such as paper, which are non-polar, it follows from the conservation of angular momentum that the stress tensor is symmetric: $\sigma_{ij} = \sigma_{ji}$. The stress vector can be decomposed into two parts: normal stress and shear stress. Normal stress, defined as

$$\sigma_n = (\boldsymbol{t}, \boldsymbol{n}) = (\boldsymbol{n}, \mathcal{T}\boldsymbol{n}), \tag{2.8}$$

acting normal to the area element, causes the compression (positive) or expansion (negative) of a volume element in the direction of the normal. Shear stresses, defined as

$$\boldsymbol{\tau} = \boldsymbol{t} - \sigma_n \boldsymbol{n} = \mathcal{T}\boldsymbol{n} = \mathcal{T}\boldsymbol{n} - (\boldsymbol{n}, \mathcal{T}\boldsymbol{n})\boldsymbol{n}, \tag{2.9}$$

are perpendicular to normal stress. They act in the plane of the contact surface between the two volume elements and cause shear deformation. With respect to a Cartesian coordinate system, $\{x_1, x_2, x_3\}$ the components σ_{ij} are defined as

$$\sigma_{ij} := (\boldsymbol{e}_i, \mathcal{T}\boldsymbol{e}_j) = (\boldsymbol{e}_j, \mathcal{T}\boldsymbol{e}_i), \quad (i, j) = (1, 2, 3). \tag{2.10}$$

Hence, σ_{ij} is the i-component of the stress vector $\boldsymbol{t}$ acting on a plane with outward normal in the j-direction, or, since the stress tensor is symmetric, vice versa.

2.1.5 Constitutive equations

Now that we have introduced the notions of stress and strain, we can define elasticity more rigorously. As mentioned at the start of this chapter an elastic material, which deforms because of an external influence, returns to its initial, undeformed, configuration when it is no longer exposed to this external influence. This can be expressed more precisely by stating:
A material is called elastic if the stress $\mathcal{T}$ and the (elastic) internal energy Σ at some position $\boldsymbol{x}_0$ in a

configuration $\mathcal{G}_0$ *depend only on the deformation tensor at* $\boldsymbol{x}_0$ *in configuration* $\mathcal{G}_0$, i.e.

$$\mathcal{T}(\boldsymbol{x}_0) = \mathcal{T}(\mathcal{E}(\boldsymbol{x}_0)), \quad \Sigma(\boldsymbol{x}_0) = \Sigma(\mathcal{E}(\boldsymbol{x}_0)). \tag{2.11}$$

In the case of linear elasticity theory we can relate the stress and strain by means of *Hooke's law*. We assume paper can be modeled as an orthotropic material, which means it has three mutually orthogonal planes of symmetry in the (x, y, z)-directions. The assumption of orthotropy stems from the assumption that the fibre alignment is the only factor causing anisotropy. Assuming that the fibre alignment is parallel to an edge of the sheet, we write Hooke's law as [8]

$$\begin{bmatrix} \varepsilon_{xx} \\ \varepsilon_{yy} \\ \varepsilon_{zz} \\ \varepsilon_{yz} \\ \varepsilon_{xz} \\ \varepsilon_{xy} \end{bmatrix} = \begin{bmatrix} \frac{1}{E_x} & -\frac{\nu_{yx}}{E_y} & -\frac{\nu_{zx}}{E_z} & 0 & 0 & 0 \\ -\frac{\nu_{xy}}{E_x} & \frac{1}{E_y} & -\frac{\nu_{zy}}{E_z} & 0 & 0 & 0 \\ -\frac{\nu_{xz}}{E_x} & -\frac{\nu_{yz}}{E_y} & \frac{1}{E_z} & 0 & 0 & 0 \\ 0 & 0 & 0 & \frac{1}{2G_{yz}} & 0 & 0 \\ 0 & 0 & 0 & 0 & \frac{1}{2G_{xz}} & 0 \\ 0 & 0 & 0 & 0 & 0 & \frac{1}{2G_{xy}} \end{bmatrix} \begin{bmatrix} \sigma_{xx} \\ \sigma_{yy} \\ \sigma_{zz} \\ \sigma_{yz} \\ \sigma_{xz} \\ \sigma_{xy} \end{bmatrix}. \tag{2.12}$$

Here, we introduced several material constants: $E_i, i = x, y, z$, the Young's moduli in their respective directions are measures for the tensile stiffness of the material. The shear moduli G_{ij} are measures for the shear stiffness. The Poisson ratios ν_{ij} quantify the contraction in direction j caused by the expansion in direction i. Because of Betti-Maxwell's reciprocal theorem the matrix in Hooke's law must be symmetric [8], §7.2, so we have

$$\frac{\nu_{ij}}{E_i} = \frac{\nu_{ji}}{E_j}, \qquad i \neq j. \tag{2.13}$$

Hence, of the 12 material constants in (2.12) 9 are independent of one another.

In nonlinear elasticity theory, the constitutive relation is given by

$$\mathcal{T} = \rho \mathcal{F} \frac{\partial \Sigma}{\partial \mathcal{E}} \mathcal{F}^T, \tag{2.14}$$

where ρ denotes the density and $\Sigma(\mathcal{E})$ the elastic energy density. We will use this formulation in Section 2.3.

2.1.6 Equilibrium equations

Conservation of momentum for an equilibrium state leads to the *equilibrium equations* [5]:

$$\frac{\partial \sigma_{xx}}{\partial x} + \frac{\partial \sigma_{xy}}{\partial y} + \frac{\partial \sigma_{xz}}{\partial z} + F_x = 0, \tag{2.15}$$

$$\frac{\partial \sigma_{yx}}{\partial x} + \frac{\partial \sigma_{yy}}{\partial y} + \frac{\partial \sigma_{yz}}{\partial z} + F_y = 0, \tag{2.16}$$

$$\frac{\partial \sigma_{zx}}{\partial x} + \frac{\partial \sigma_{zy}}{\partial y} + \frac{\partial \sigma_{zz}}{\partial z} + F_z = 0. \tag{2.17}$$

Here, $F_i, i = x, y, z$ represent the body forces directed in each of the directions ($[\boldsymbol{F}] = \mathrm{N/m^3}$), for example, gravity can be included in the model in this way.

To summarize the results from the past sections; the elastic body is described by 15 variables; 6 stresses, 6 strains and 3 displacements, which are related to one another by 15 equations; 6 strain-displacement relations (2.3), 6 constitutive relations expressed in Hooke's law (2.12) and the 3 equilibrium equations from this section.

2.1.7 Boundary conditions

To complete the system described by the equations in the preceding sections, we need to impose three boundary conditions on each point at the boundary in the undeformed (reference) state of the elastic body $\mathcal{G}_{\mathcal{R}}$. These boundary conditions can be of the following types [6], p. 66:

- A condition for the stress:

$$\mathcal{T}\boldsymbol{n} = \boldsymbol{t}^*, \quad \boldsymbol{x} \in \partial\mathcal{G}_{\mathcal{R}}, \tag{2.18}$$

- A condition for the displacements:

$$\mathcal{D}(\boldsymbol{u}) = \boldsymbol{u}^*, \quad \boldsymbol{x} \in \partial\mathcal{G}_{\mathcal{R}}, \tag{2.19}$$

  where $\mathcal{D}$ is some (differential) operator, and $\boldsymbol{t}^*$ and $\boldsymbol{u}^*$ are precribed vector functions at $\partial\mathcal{G}_{\mathcal{R}}$

- Combinations of the two conditions.

2.2 Kirchhoff plate theory

In the case of a thin plate, i.e. one dimension of the body being small compared to the other two, we can employ the so-called *Kirchhoff plate theory* to describe the deformations. The small dimension is called thickness, denoted by $2h$. Letting L be a typical dimension of the length and width, we posit $h \ll L$. Kirchhoff plate theory reduces the three-dimensional problem to two dimensions by approximating around the so-called midplane: the (x, y)-plane at $z = 0$, the middle of the plate. Hence, the x- and y-coordinate are in the midplane and the z-coordinate ($-h < z < h$) is normal to the midplane. We will sometimes refer to the z-direction as the vertical direction. To employ this theory, we need to impose a number of assumptions, known as the Kirchhoff hypotheses, [8], §1.3:

1. The material of the plate is elastic and homogeneous.

2. The plate is initially flat.

3. The deflection, i.e. the vertical component of the displacement vector, of the midplane is small compared to the thickness of the plate ($w \ll h$). The magnitude of the, dimensionless, slope of the deflected surface is therefore small and the square of the slope is considered a negligible quantity.

4. Normals to the original configuration of the plate remain straight and normal to the plate after deformation. This means that the vertical shear strains ε_{xz} and ε_{yz} are considered negligible.

5. The stress normal to the midplane σ_{zz} is small compared to the other stress components and may be neglected in the stress-strain relations.

6. Since the displacements of the plate are small, it is assumed that bending keeps the midplane unstrained; this means that the in-plane strains are only due to stretching.

Let u_x, u_y and u_z denote the components of the displacements of the plate in $x-, y-$, and $z-$direction, respectively, and u, v, and w the corresponding displacements of the midplane, initially at $z = 0$. This leads to the following representation of the displacements:

$$u_x(x, y, z) = u(x, y) - z\frac{\partial w(x, y)}{\partial x}, \quad u_y(x, y, z) = v(x, y) - z\frac{\partial w(x, y)}{\partial y}, \quad u_z(x, y, z) = w(x, y). \tag{2.20}$$

which is essentially a first-order Taylor approximation around the midplane. We follow the assumptions to reduce Hooke's law (2.12) to

$$\begin{bmatrix} \varepsilon_{xx} \\ \varepsilon_{yy} \\ \varepsilon_{xy} \end{bmatrix} = \begin{bmatrix} \frac{1}{E_x} & -\frac{\nu_{yx}}{E_y} & 0 \\ -\frac{\nu_{xy}}{E_x} & \frac{1}{E_y} & 0 \\ 0 & 0 & \frac{1}{2G_{xy}} \end{bmatrix} \begin{bmatrix} \sigma_{xx} \\ \sigma_{yy} \\ \sigma_{xy} \end{bmatrix}. \tag{2.21}$$

In the next two sections we make a distinction between stretching and bending of the plate and derive equations that describe these deformations separately. These two types of deformations will be coupled in Section 2.4 to model large out-of-plane deformations.

2.2.1 Stretching

To derive an equation describing the stresses relating to stretching of a plate, we consider a plate subject to an in-plane force at its edges, which causes it to stretch in the (x, y)-plane without bending, i.e. $w = 0$. To be able to compose global force relations, we define global forces acting in the midplane. For the forces acting in the plane, we find ($[N_{ij}]$ =N/m)

$$\begin{bmatrix} N_{xx} \\ N_{yy} \\ N_{xy} \end{bmatrix} = \int_{-h}^{h} \begin{bmatrix} \sigma_{xx} \\ \sigma_{yy} \\ \sigma_{xy} \end{bmatrix} dz. \tag{2.22}$$

To obtain the force balances in the $x-$ and $y-$direction we integrate the equilibrium equations (2.15), (2.16) over the thickness of the plate and use (2.22) to find:

$$\begin{aligned} \frac{\partial N_{xx}}{\partial x} + \frac{\partial N_{xy}}{\partial y} &= 0, \\ \frac{\partial N_{xy}}{\partial x} + \frac{\partial N_{yy}}{\partial y} &= 0. \end{aligned} \tag{2.23}$$

These equations are trivially satisfied by introducing the so-called Airy stress function $\varphi(x, y)$, [8], Chapter 1:

$$\frac{\partial^2 \varphi}{\partial y^2} = \sigma_{xx} = \frac{N_{xx}}{2h}, \qquad \frac{\partial^2 \varphi}{\partial x \partial y} = -\sigma_{xy} = -\frac{N_{xy}}{2h}, \qquad \frac{\partial^2 \varphi}{\partial x^2} = \sigma_{yy} = \frac{N_{yy}}{2h}. \tag{2.24}$$

Using Hooke's law (2.21) to express the relevant compatibility equation (2.6) in terms of stresses, and writing this in terms of the Airy stress function, we eventually arrive at:

$$\begin{aligned} \frac{\partial^2 \varepsilon_{xx}}{\partial y^2} + \frac{\partial^2 \varepsilon_{yy}}{\partial x^2} - 2\frac{\partial^2 \varepsilon_{xy}}{\partial x \partial y} &= \frac{1}{E_x}\frac{\partial^2 \sigma_{xx}}{\partial y^2} - \frac{\nu_{yx}}{E_y}\frac{\partial^2 \sigma_{yy}}{\partial y^2} - \frac{\nu_{xy}}{E_x}\frac{\partial^2 \sigma_{xx}}{\partial x^2} + \frac{1}{E_y}\frac{\partial^2 \sigma_{yy}}{\partial x^2} - \frac{1}{G_{xy}}\frac{\partial^2 \sigma_{xy}}{\partial x \partial y} \\ &= \frac{1}{E_y}\frac{\partial^4 \varphi}{\partial x^4} + \left(2\frac{\nu_{xy}}{E_x} + \frac{1}{G_{xy}}\right)\frac{\partial^4 \varphi}{\partial x^2 \partial y^2} + \frac{1}{E_x}\frac{\partial^4 \varphi}{\partial y^4} = 0. \end{aligned} \tag{2.25}$$

This equation describes the in-plane deformations resulting from in-plane stresses.

2.2.2 Bending

In the case of pure bending we have $u = v = 0$, such that we find for the strains

$$\varepsilon_{xx} = -z\frac{\partial^2 w}{\partial x^2}, \quad \varepsilon_{xy} = -z\frac{\partial^2 w}{\partial x \partial y}, \quad \varepsilon_{yy} = -z\frac{\partial^2 w}{\partial y^2}. \tag{2.26}$$

Inverting (2.21) yields

$$\begin{aligned}
\sigma_{xx} &= \frac{E_x}{1-\nu_{xy}\nu_{yx}}\Big(\varepsilon_{xx}+\nu_{yx}\varepsilon_{yy}\Big) = -\frac{zE_x}{1-\nu_{xy}\nu_{yx}}\Big(\frac{\partial^2 w}{\partial x^2}+\nu_{yx}\frac{\partial^2 w}{\partial y^2}\Big),\\
\sigma_{yy} &= \frac{E_y}{1-\nu_{xy}\nu_{yx}}\Big(\nu_{xy}\varepsilon_{xx}+\varepsilon_{yy}\Big) = -\frac{zE_y}{1-\nu_{xy}\nu_{yx}}\Big(\nu_{xy}\frac{\partial^2 w}{\partial x^2}+\frac{\partial^2 w}{\partial y^2}\Big),\\
\sigma_{xy} &= 2G_{xy}\varepsilon_{xy} = -2zG_{xy}\frac{\partial^2 w}{\partial x\partial y}.
\end{aligned} \tag{2.27}$$

Note that all the stresses due to bending depend linearly upon z. We introduce the bending moments M_{xx}, M_{yy} and twisting moment M_{xy}, ($[M_{ij}]$ =N), using these expressions:

$$\begin{bmatrix} M_{xx}\\ M_{yy}\\ M_{xy}\end{bmatrix} = \int_{-h}^{h}\begin{bmatrix}\sigma_{xx}\\ \sigma_{yy}\\ \sigma_{xy}\end{bmatrix} z dz = -\frac{2h^3}{3}\begin{bmatrix} \dfrac{E_x}{1-\nu_{xy}\nu_{yx}}\left(\dfrac{\partial^2 w}{\partial x^2}+\nu_{yx}\dfrac{\partial^2 w}{\partial y^2}\right)\\[2ex] \dfrac{E_y}{1-\nu_{xy}\nu_{yx}}\left(\nu_{xy}\dfrac{\partial^2 w}{\partial x^2}+\dfrac{\partial^2 w}{\partial y^2}\right)\\[2ex] 2G_{xy}\dfrac{\partial^2 w}{\partial x\partial y}\end{bmatrix}. \tag{2.28}$$

We note that, because the stress tensor is symmetric we need not introduce M_{yx}.

We define the shear forces as ($[Q_i]$ =N/m):

$$\begin{bmatrix} Q_x\\ Q_y\end{bmatrix} = \int_{-h}^{h}\begin{bmatrix}\sigma_{xz}\\ \sigma_{yz}\end{bmatrix} dz. \tag{2.29}$$

Although the shears ε_{xz} and ε_{yz} are assumed zero (the fourth Kirchhoff assumption), and hence also the shear stresses σ_{xz} and σ_{yz}, according to Hooke's law, the shear forces Q_x and Q_y are not taken zero, and included in the global equilibrium equations. This seems somewhat conflicting, but it has shown to be consistent within Kirchhoff's thin plate theory [8].

We now consider a plate subject to a vertical load per unit area $q(x,y)$ ($[q]$ =N/m^2). We compose global force balances for this situation by multiplying equations (2.15) and (2.16) by z and integrating them, along with (2.17). Expressing this in terms of the shear force and bending and twisting moments, we obtain

$$\begin{aligned}
\frac{\partial M_{xx}}{\partial x}+\frac{\partial M_{xy}}{\partial y} &= Q_x,\\
\frac{\partial M_{xy}}{\partial x}+\frac{\partial M_{yy}}{\partial y} &= Q_y,\\
\frac{\partial Q_x}{\partial x}+\frac{\partial Q_y}{\partial y} &= q.
\end{aligned} \tag{2.30}$$

Eliminating Q_x, Q_y from these expressions, we find

$$\frac{\partial^2 M_{xx}}{\partial x^2}+2\frac{\partial^2 M_{xy}}{\partial x\partial y}+\frac{\partial^2 M_{yy}}{\partial y^2} = q. \tag{2.31}$$

Using equations (2.27) and (2.28), we obtain an expression for the deflection w resulting from the load q:

$$\frac{2h^3}{3}\left(\frac{E_x}{1-\nu_{xy}\nu_{yx}}\frac{\partial^4 w}{\partial x^4}+2\left(\frac{\nu_{yx}E_x}{1-\nu_{xy}\nu_{yx}}+G_{xy}\right)\frac{\partial^4 w}{\partial x^2\partial y^2}+\frac{E_y}{1-\nu_{xy}\nu_{xy}}\frac{\partial^4 w}{\partial y^4}\right) = q. \tag{2.32}$$

This equation describes the out-of-plane deformations resulting from an external force, provided they remain small.

2.2.3 Moisture-induced stresses

In the literature often the deformations resulting from a rise in temperature are discussed [7], [8]. The effect of water uptake is modeled in the same manner, by adding a term to Hooke's law (2.21):

$$\begin{bmatrix} \varepsilon_{xx} \\ \varepsilon_{yy} \\ \varepsilon_{xy} \end{bmatrix} = \begin{bmatrix} \frac{1}{E_x} & -\frac{\nu_{yx}}{E_y} & 0 \\ -\frac{\nu_{xy}}{E_x} & \frac{1}{E_y} & 0 \\ 0 & 0 & \frac{1}{2G_{xy}} \end{bmatrix} \begin{bmatrix} \sigma_{xx} \\ \sigma_{yy} \\ \sigma_{xy} \end{bmatrix} + \begin{bmatrix} \varepsilon^h_{xx} \\ \varepsilon^h_{yy} \\ 0 \end{bmatrix}. \tag{2.33}$$

where $\varepsilon^h_{xx} = \beta_x \chi(x,y)$ and $\varepsilon^h_{yy} = \beta_y \chi(x,y)$ denote the water-induced strains. The change in moisture content is $\chi(x,y)$ and $\beta_i, i = x, y$, denotes the so-called hygroexpansivity coefficient, which quantifies the relative growth of the fibres per percent increase of moisture content.

2.3 Linearization about an intermediate state

To model large out-of-plane displacements, as occur in the case of moisturized paper, we need a nonlinear version of the equilibrium equations given in Section 2.1.6. To this end, we consider a plate deforming from an initial configuration $\mathcal{G}_\mathcal{R}$ to a configuration $\mathcal{G}$, through an intermediate configuration $\mathcal{G}_\mathcal{I}$:

$$\boldsymbol{X} \in \mathcal{G}_\mathcal{R} \rightarrow \boldsymbol{\xi} := \boldsymbol{X} + \boldsymbol{u}^0 \in \mathcal{G}_\mathcal{I} \rightarrow \boldsymbol{x} := \boldsymbol{\xi} + \boldsymbol{u} \in \mathcal{G}_\mathcal{R}. \tag{2.34}$$

We assume the second deformation to be small, which we quantify by $||\nabla \boldsymbol{u}|| = \varepsilon \ll 1$. Keeping the nonlinear theory from Section 2.1.5 and (2.14) in mind, we find:

$$\mathcal{F}^0 = \frac{\partial \xi}{\partial \boldsymbol{X}}, \quad \mathcal{E}^0 = \frac{1}{2}\Big(\mathcal{F}^{0^T}\mathcal{F}^0 - \mathcal{I}\Big), \quad \sigma^0 = \rho^0 \mathcal{F}^0 \Big(\frac{\partial \Sigma}{\partial \mathcal{E}}\Big)^0 \mathcal{F}^{0^T}. \tag{2.35}$$

Here we denote the intermediate state of the variables by a superscript ^{0}. The equilibrium equation for the intermediate state reads

$$\nabla \cdot \sigma^0 + F^0_i = 0, \tag{2.36}$$

where F^0_i denotes the external body force. Using this notation, we obtain the deformation gradient for the composition of the two deformations

$$\mathcal{F} = \frac{\partial \boldsymbol{x}}{\partial \boldsymbol{X}} = \frac{\partial \boldsymbol{\xi}}{\partial \boldsymbol{X}} + \frac{\partial \boldsymbol{u}}{\partial \boldsymbol{X}} = \frac{\partial \boldsymbol{\xi}}{\partial \boldsymbol{X}} + \frac{\partial \boldsymbol{u}}{\partial \boldsymbol{\xi}} \frac{\partial \boldsymbol{\xi}}{\partial \boldsymbol{X}} = \mathcal{F}^0 + \frac{\partial \boldsymbol{u}}{\partial \boldsymbol{\xi}} \mathcal{F}^0. \tag{2.37}$$

The change in density can be expressed in terms of the deformation gradient. Denoting the density in successively $\mathcal{G}_R, \mathcal{G}_I, \mathcal{G}$ by ρ_0, ρ^0, ρ, we have:

$$\rho^0 = \frac{\rho_0}{\mathcal{J}^0}, \quad \rho = \frac{\rho_0}{\mathcal{J}} = \rho^0 \frac{\mathcal{J}^0}{\mathcal{J}}, \tag{2.38}$$

where $\mathcal{J} = \det \mathcal{F}, \mathcal{J}^0 = \det \mathcal{F}^0$. We approximate

$$\mathcal{J} = \det \mathcal{F} = \det\Big(\mathcal{F}^0 + \frac{\partial \boldsymbol{u}}{\partial \boldsymbol{\xi}} \mathcal{F}^0\Big) \doteq \mathcal{J}^0 \left(1 + \operatorname{tr}\Big(\frac{\partial \boldsymbol{u}}{\partial \boldsymbol{\xi}}\Big)\right). \tag{2.39}$$

Linearizing (2.14) , we arrive at the constitutive equation:

$$\sigma = \rho \mathcal{F} \frac{\partial \Sigma}{\partial \mathcal{E}} \mathcal{F}^T = \frac{\rho^0}{1 + \operatorname{tr}\left(\frac{\partial \boldsymbol{u}}{\partial \boldsymbol{\xi}}\right)} \left(\mathcal{F}^0 + \frac{\partial \boldsymbol{u}}{\partial \boldsymbol{\xi}} \mathcal{F}^0\right) \left[\Big(\frac{\partial \Sigma}{\partial \mathcal{E}}\Big)^0 + \Big(\frac{\partial^2 \Sigma}{\partial \mathcal{E} \partial \mathcal{E}}\Big)^0 \Big(\mathcal{E} - \mathcal{E}^0\Big)\right] \left(\mathcal{F}^{0^T} + \frac{\partial \boldsymbol{u}}{\partial \boldsymbol{\xi}} \mathcal{F}^{0^T}\right). \tag{2.40}$$

or component-wise:

$$\begin{aligned}\sigma_{ij} &= \Big(\rho^0\Big(\frac{\partial\Sigma}{\partial\varepsilon_{\alpha\beta}}\Big)^0 F^0_{i\alpha}F^0_{j\beta}\Big) + \Big(\rho^0\Big(\frac{\partial^2\Sigma}{\partial\varepsilon_{\alpha\beta}\partial\varepsilon_{\gamma\delta}}\Big)^0 F_{i\alpha}F_{j\beta}\Big(\varepsilon_{\gamma\delta}-\varepsilon^0_{\gamma\delta}\Big)\Big)\\ &\quad + \rho^0\Big(\frac{\partial\Sigma}{\partial\varepsilon_{\alpha\beta}}\Big)^0\Big(-u_{k,k}F^0_{i\alpha}F^0_{j\beta}+u_{i,l}F^0_{l\alpha}F^0_{j\beta}+u_{j,l}F^0_{i\alpha}F^0_{l\beta}\Big)\\ &= T^0_{ij}+t_{ij}+\Big(-\delta_{kl}T^0_{ij}+\delta_{ik}T^0_{lj}+\delta_{jk}T^0_{il}\Big)u_{k,l},\end{aligned} \tag{2.41}$$

with

$$T^0_{ij}=\rho^0\left(\frac{\partial\Sigma}{\partial\varepsilon_{\alpha\beta}}\right)^0 F^0_{i\alpha}F^0_{j\beta},\quad t_{ij}=\rho^0\left(\frac{\partial^2\Sigma}{\partial\varepsilon_{\alpha\beta}\partial\varepsilon_{\gamma\delta}}\right)^0 F^0_{i\alpha}F^0_{j\beta}\left(\varepsilon_{\gamma\delta}-\varepsilon^0_{\gamma\delta}\right). \tag{2.42}$$

If we substitute

$$\varepsilon_{\gamma\delta}-\varepsilon^0_{\gamma\delta}=\frac{1}{2}(u_{k,l}+u_{l,k})F^0_{k\gamma}F^0_{l\delta},\quad c_{ijkl}:=\rho^0\left(\frac{\partial^2\Sigma}{\partial\varepsilon_{\alpha\beta}\partial\varepsilon_{\gamma\delta}}\right)^0, \tag{2.43}$$

into (2.41) we recover the linear version of the constitutive equations, Hooke's law

$$t_{ij}=c_{ijkl}\varepsilon_{kl}. \tag{2.44}$$

Finally with (2.41) we rewrite the equilibrium equations, yielding:

$$\begin{aligned}\frac{\partial\sigma_{ij}}{\partial x_j}+F_i &= \frac{\partial\sigma_{ij}}{\partial\xi_k}\frac{\partial\xi_k}{\partial x_j}+F_i=\frac{\partial}{\partial\xi_k}\left(T^0_{ij}+(\sigma_{ij}-T^0_{ij})\right)(\delta_{kj}-u_{k,j})+F_i\\ &= \frac{\partial T^0_{ij}}{\partial\xi_j}+\frac{\partial}{\partial\xi_j}(\sigma_{ij}-T^0_{ij})-\frac{\partial T^0_{ij}}{\partial\xi_k}u_{k,j}+t_{ij,j}+F_i\\ &= -(T^0_{ij}u_{k,k})_{,j}+(T^0_{jl}u_{i,l})_{,j}+(T^0_{il}u_{j,k})_{,j}-T^0_{ij,k}u_{k,j}+t_{ij,j}+F_i\\ &= -T^0_{ij,j}u_{k,k}-T^0_{ij}u_{kj,j}+T^0_{lj,j}u_{i,l}+T^0_{lj}u_{i,jl}+T^0_{il,j}u_{j,l}+T^0_{il}u_{j,jl}-T^0_{ij,k}u_{k,j}+t_{ij,j}+F_i\\ &= t_{ij,j}+T^0_{jk}u_{i,jk}+F_i=0.\end{aligned} \tag{2.45}$$

This linearized version of the equilibrium equations will be used in the next section to derive the equations coupling bending and stretching.

2.4 Von Kármán theory for large displacements

2.4.1 Assumptions

To model the situation of a sheet of paper deforming under the influence of a change in moisture content we need to adapt the Kirchhoff model as discussed in Section 2.2. Since in the situation at hand buckling will occur and the deflections out of the plane will not be negligible compared with the thickness of the paper sheet in the post-buckling range of moisture contents, we need to reconsider the assumptions made in Section 2.2. The third and the sixth assumptions are no longer valid. We will assume a new scaling, using the small parameter $\delta = h/L$:

$$\frac{w}{h}=\mathcal{O}(1),\qquad \frac{w}{L}=\mathcal{O}(\delta),\qquad \left(\frac{u}{L},\frac{v}{L}\right)=\mathcal{O}(\delta^2). \tag{2.46}$$

Neglecting terms of $\mathcal{O}(\delta^3)$, we obtain from (2.3) and (2.20) the representation for the strains:

$$\begin{aligned}
\varepsilon_{xx} &= \frac{\partial u}{\partial x} + \frac{1}{2}\left(\frac{\partial w}{\partial x}\right)^2 - z\frac{\partial^2 w}{\partial x^2},\\
\varepsilon_{xy} &= \frac{1}{2}\left(\frac{\partial u}{\partial y} + \frac{\partial v}{\partial x} + \frac{\partial w}{\partial x}\frac{\partial w}{\partial y}\right) - z\frac{\partial^2 w}{\partial x \partial y},\\
\varepsilon_{yy} &= \frac{\partial v}{\partial y} + \frac{1}{2}\left(\frac{\partial w}{\partial y}\right)^2 - z\frac{\partial^2 w}{\partial y^2}.
\end{aligned} \tag{2.47}$$

We note that the strains in (2.47) can be decomposed into a part independent of z and a part that depends linearly on z. The independent parts are the in-plane deformations due to stretching and the linearly dependent parts are the out-of-plane deformation due to bending. The in-plane strains now depend on w, which couples the bending and stretching in this theory.

Next we will derive equations for the stretching and bending of plates in the model under consideration, using an approach similar to the one followed in Sections 2.2.1 and 2.2.2.

2.4.2 Stretching

We invert Hooke's law (2.33) and use (2.47) to express the stresses in terms of the displacements, resulting in

$$\begin{aligned}
\sigma_{xx} &= \frac{E_x}{1-\nu_{xy}\nu_{yx}}\left(\varepsilon_{xx} - \varepsilon^h_{xx} + \nu_{yx}(\varepsilon_{yy} - \varepsilon^h_{yy})\right)\\
&= \frac{E_x}{1-\nu_{xy}\nu_{yx}}\left(\left(\frac{\partial u}{\partial x} - z\frac{\partial^2 w}{\partial x^2} + \frac{1}{2}\left(\frac{\partial w}{\partial x}\right)^2 - \varepsilon^h_{xx}\right) + \nu_{yx}\left(\frac{\partial u}{\partial y} - z\frac{\partial^2 w}{\partial y^2} + \frac{1}{2}\left(\frac{\partial w}{\partial y}\right)^2 - \varepsilon^h_{yy}\right)\right),\\
\sigma_{yy} &= \frac{E_y}{1-\nu_{xy}\nu_{yx}}\left(\nu_{xy}(\varepsilon_{xx} - \varepsilon^h_{xx}) + \varepsilon_{yy} - \varepsilon^h_{yy}\right)\\
&= \frac{E_y}{1-\nu_{xy}\nu_{yx}}\left(\nu_{xy}\left(\frac{\partial u}{\partial x} - z\frac{\partial^2 w}{\partial x^2} + \frac{1}{2}\left(\frac{\partial w}{\partial x}\right)^2 - \varepsilon^h_{xx}\right) + \left(\frac{\partial u}{\partial y} - z\frac{\partial^2 w}{\partial y^2} + \frac{1}{2}\left(\frac{\partial w}{\partial y}\right)^2 - \varepsilon^h_{yy}\right)\right),\\
\sigma_{xy} &= 2G_{xy}\varepsilon_{xy} = G_{xy}\left(\frac{\partial u}{\partial y} + \frac{\partial v}{\partial x} + \frac{\partial w}{\partial x}\frac{\partial w}{\partial y} - 2z\frac{\partial^2 w}{\partial x \partial y}\right).
\end{aligned} \tag{2.48}$$

We decompose the stresses into the in-plane part and the out-of-plane part as follows: $\sigma_{ij} = \sigma^{(0)}_{ij}(x,y) + z\sigma^{(1)}_{ij}(x,y), (i,j) \in (x,y)$. We proceed as in Section 2.2.1 and integrate the equilibrium equations (2.15), (2.16) over the thickness of the plate, to obtain

$$\begin{aligned}
\int_{-h}^{h}\left(\frac{\partial \sigma^{(0)}_{xx}}{\partial x} + \frac{\partial \sigma^{(0)}_{xy}}{\partial y}\right)\mathrm{d}z &= \int_{-h}^{h}\left(\frac{\partial \sigma^{(0)}_{xx}}{\partial x} + z\frac{\partial \sigma^{(1)}_{xx}}{\partial x} + \frac{\partial \sigma^{(0)}_{xy}}{\partial y} + z\frac{\partial \sigma^{(1)}_{xy}}{\partial y}\right)\mathrm{d}z\\
&= \int_{-h}^{h}\left(\frac{\partial \sigma_{xx}}{\partial x} + \frac{\partial \sigma_{xy}}{\partial y}\right)\mathrm{d}z = \frac{\partial N_{xx}}{\partial x} + \frac{\partial N_{xy}}{\partial y} = 0,
\end{aligned} \tag{2.49}$$

$$\begin{aligned}
\int_{-h}^{h}\left(\frac{\partial \sigma^{(0)}_{xy}}{\partial x} + \frac{\partial \sigma^{(0)}_{yy}}{\partial y}\right)\mathrm{d}z &= \int_{-h}^{h}\left(\frac{\partial \sigma^{(0)}_{xy}}{\partial x} + z\frac{\partial \sigma^{(1)}_{xy}}{\partial x} + \frac{\partial \sigma^{(0)}_{yy}}{\partial y} + z\frac{\partial \sigma^{(1)}_{yy}}{\partial y}\right)\mathrm{d}z\\
&= \int_{-h}^{h}\left(\frac{\partial \sigma_{xy}}{\partial x} + \frac{\partial \sigma_{yy}}{\partial y}\right)\mathrm{d}z = \frac{\partial N_{xy}}{\partial x} + \frac{\partial N_{yy}}{\partial y} = 0.
\end{aligned} \tag{2.50}$$

To satisfy these global equilibrium equations, we again use the Airy stress function (2.24). To derive the equation for the stretching of the plate, we substitute (2.47) into the fourth compatibility equation (2.6) and

evaluate this at $z = 0$, yielding

$$\left[\frac{\partial^2 \varepsilon_{xx}}{\partial y^2} - 2\frac{\partial^2 \varepsilon_{xy}}{\partial x \partial y} + \frac{\partial^2 \varepsilon_{yy}}{\partial x^2}\right]_{z=0} = \left(\frac{\partial^2 w}{\partial x \partial y}\right)^2 - \frac{\partial^2 w}{\partial x^2}\frac{\partial^2 w}{\partial y^2}. \tag{2.51}$$

Writing this in terms of the Airy stress function while keeping in mind Hooke's law including hygro-expansion, (2.33), we eventually arrive at

$$\frac{\partial^2 \varepsilon^h_{xx}}{\partial y^2} + \frac{\partial^2 \varepsilon^h_{yy}}{\partial x^2} + \frac{1}{E_y}\frac{\partial^4 \varphi}{\partial x^4} + \left(\frac{1}{G_{xy}} - 2\frac{\nu_{xy}}{E_x}\right)\frac{\partial^4 \varphi}{\partial x^2 \partial y^2} + \frac{1}{E_x}\frac{\partial^4 \varphi}{\partial y^4} = \left(\frac{\partial^2 w}{\partial x \partial y}\right)^2 - \frac{\partial^2 w}{\partial x^2}\frac{\partial^2 w}{\partial y^2}. \tag{2.52}$$

This constitutes our first equation for the post-buckling theory of a wetted sheet of paper describing the stresses resulting from a rise in moisture content.

2.4.3 Bending

To derive the equation for large deformation bending we start with the linearized equilibrium equation (2.45),

$$t_{ij,j} + T^0_{ij} u_{i,jk} + F_i = 0. \tag{2.53}$$

Here we have for T^0_{jk}, being the intermediate stresses due to the stretching of the plate,

$$T^0_{11} = \frac{N_{xx}}{2h}, \quad T^0_{12} = \frac{N_{xy}}{2h}, \quad T^0_{22} = \frac{N_{yy}}{2h}, \tag{2.54}$$

with the N_{ij}'s as found in the preceding section. For u_i we take (2.20) with $u = v = 0$. Moreover, we take only a vertical load, so $F_x = F_y = 0$. Finally, we neglect all terms of $\mathcal{O}(\delta^3)$, since the resulting equations are of order $\mathcal{O}(\delta^2)$. Taking all of this into account, we arrive at:

$$\begin{aligned}
&\frac{\partial t_{xx}}{\partial x} + \frac{\partial t_{xy}}{\partial y} + \frac{\partial t_{xz}}{\partial z} - \frac{z}{2h}\left(N_{xx}\frac{\partial^3 w}{\partial x^3} + N_{xy}\frac{\partial^3 w}{\partial x^2 \partial y} + N_{yy}\frac{\partial^3 w}{\partial x \partial y^2}\right) = 0,\\
&\frac{\partial t_{xy}}{\partial x} + \frac{\partial t_{yy}}{\partial y} + \frac{\partial t_{yz}}{\partial z} - \frac{z}{2h}\left(N_{xx}\frac{\partial^3 w}{\partial x^2 \partial y} + N_{xy}\frac{\partial^3 w}{\partial x \partial y^2} + N_{yy}\frac{\partial^3 w}{\partial y^3}\right) = 0,\\
&\frac{\partial t_{xz}}{\partial x} + \frac{\partial t_{yz}}{\partial y} + \frac{\partial t_{zz}}{\partial z} - \frac{z}{2h}\left(N_{xx}\frac{\partial^2 w}{\partial x^2} + N_{xy}\frac{\partial^2 w}{\partial x \partial y} + N_{yy}\frac{\partial^2 w}{\partial y^2}\right) + F_z = 0.
\end{aligned} \tag{2.55}$$

From the first equation of (2.55), considering that the last term is of $\mathcal{O}(\delta^3)$, we obtain after multiplication with z and integration over the thickness, the global moment equation (analogous to (2.30)):

$$\int_{-h}^{h}\left(z\frac{\partial t_{xx}}{\partial x} + z\frac{\partial t_{xy}}{\partial y} + z\frac{\partial t_{xz}}{\partial z}\right)\mathrm{d}z = \frac{\partial M_{xx}}{\partial x} + \frac{\partial M_{xy}}{\partial y} - Q_x = 0. \tag{2.56}$$

Analogously, we obtain from the second equation of (2.55) the moment equation in the y-direction:

$$\frac{\partial M_{xy}}{\partial x} + \frac{\partial M_{yy}}{\partial y} - Q_y = 0. \tag{2.57}$$

Integrating the third part of equation (2.55) over the thickness, we arrive at the global equation for the shear forces, in the form (note that here the last term is of order $\mathcal{O}(\delta^2)$)

$$\int_{-h}^{h}\left(\frac{\partial t_{xz}}{\partial x} + \frac{\partial t_{yz}}{\partial y} + \frac{\partial t_{zz}}{\partial z} - \frac{z}{2h}\left(N_{xx}\frac{\partial^2 w}{\partial x^2} + N_{xy}\frac{\partial^2 w}{\partial x \partial y} + N_{yy}\frac{\partial^2 w}{\partial y^2}\right) + F_z\right)\mathrm{d}z = 0 \tag{2.58}$$

Leading to

$$\frac{\partial Q_x}{\partial x} + \frac{\partial Q_y}{\partial y} = q + N_{xx}\frac{\partial^2 w}{\partial x^2} + 2N_{xy}\frac{\partial^2 w}{\partial x \partial y} + N_{yy}\frac{\partial^2 w}{\partial y^2}, \tag{2.59}$$

where

$$q = q(x,y) = \int_{-h}^{h} F_z(x,y)\mathrm{d}z + t_{zz}\Big]_{-h}^{h}. \tag{2.60}$$

With (2.56), (2.28) and (2.49) we express the shear forces in terms of the displacements, keeping in mind that the terms with an odd power of z will cancel in the integrals, to obtain

$$\begin{aligned}
\frac{\partial Q_x}{\partial x} &= \frac{\partial^2 M_{xx}}{\partial x^2} + \frac{\partial^2 M_{xy}}{\partial x \partial y} \\
&= \int_{-h}^{h} z\left(\frac{\partial^2 \sigma_{xx}}{\partial x^2} + \frac{\partial^2 \sigma_{xy}}{\partial x \partial y}\right)\mathrm{d}z = \int_{-h}^{h} z\left(\frac{\partial^2 \sigma_{xx}^{(1)}}{\partial x^2} + \frac{\partial^2 \sigma_{xy}^{(1)}}{\partial x \partial y}\right)\mathrm{d}z \\
&= \int_{-h}^{h} z\left(\frac{E_x}{1-\nu_{xy}\nu_{yx}}\left(-z\frac{\partial^4 w}{\partial x^4} - \frac{\partial^2 \varepsilon_{xx}^h}{\partial x^2} - \nu_{yx}\left(\frac{\partial^4 w}{\partial x^2 \partial y^2}\frac{\partial^2 \varepsilon_{yy}^h}{\partial y^2}\right)\right) - zG_{xy}\frac{\partial^4 w}{\partial x^2 \partial y^2}\right) \\
&= -\frac{2h^3 E_x}{3(1-\nu_{xy}\nu_{yx})}\left(\frac{\partial^4 w}{\partial x^4} + \nu_{yx}\left(\frac{\partial^4 w}{\partial x^2 \partial y^2}\right)\right) - \frac{2h^3}{3}G_{xy}\frac{\partial^4 w}{\partial x^2 \partial y^2} \\
&= -\frac{2h^3}{3}\left(\frac{E_x}{1-\nu_{xy}\nu_{yx}}\frac{\partial^4 w}{\partial x^4} + \left(\frac{\nu_{yx}E_x}{1-\nu_{xy}\nu_{yx}} + G_{xy}\right)\frac{\partial^4 w}{\partial x^2 \partial y^2}\right).
\end{aligned} \tag{2.61}$$

Analogously we derive

$$\frac{\partial Q_y}{\partial y} = -\frac{2h^3}{3}\left(\frac{E_y}{1-\nu_{xy}\nu_{yx}}\frac{\partial^4 w}{\partial y^4} + \left(\frac{\nu_{xy}E_y}{1-\nu_{xy}\nu_{yx}} + G_{xy}\right)\frac{\partial^4 w}{\partial x^2 \partial y^2}\right). \tag{2.62}$$

Combining the expressions for the shear forces (2.61) and (2.62) with the global expression (2.59), and using the Airy stress function (2.24), we obtain

$$\begin{aligned}
\frac{2h^3}{3}\left(\frac{E_y}{1-\nu_{xy}\nu_{yx}}\frac{\partial^4 w}{\partial x^4} + 2\left(\frac{\nu_{yx}E_x}{1-\nu_{xy}\nu_{yx}} + G_{xy}\right)\frac{\partial^4 w}{\partial x^2 \partial y^2}\frac{E_y}{1-\nu_{xy}\nu_{yx}}\frac{\partial^4 w}{\partial y^4}\right) \\
= q(x,y) + 2h\left(\frac{\partial^2 \varphi}{\partial x^2}\frac{\partial^2 w}{\partial y^2} + \frac{\partial^2 \varphi}{\partial y^2}\frac{\partial^2 w}{\partial x^2} - 2\frac{\partial^2 \varphi}{\partial x \partial y}\frac{\partial^2 w}{\partial x \partial y}\right),
\end{aligned} \tag{2.63}$$

which constitutes the second equation for our post-buckling model. The *Föppl-Von Kármán equations*; (2.52) and (2.63) form the equations for the two unknowns $\varphi(x,y)$ and $w(x,y)$ and thus, apart from the still needed boundary conditions, this completes our post-buckling model.

2.4.4 Boundary conditions

We consider a rectangular plate with Cartesian coordinates $\{x,y,z\} \in \{[0,a],[0,b],[-h,h]\}$. In the literature often conditions of simply supported or clamped edges are imposed, but in our case we only consider freely movable boundaries. Thus the boundary conditions for the stresses are:

$$\text{At } x = 0, a: \qquad \sigma_{xx} = \sigma_{xy} = 0. \tag{2.64}$$

$$\text{At } y = 0, b: \qquad \sigma_{xy} = \sigma_{yy} = 0. \tag{2.65}$$

The boundary conditions for the displacements are a little more complicated. At the edges at $x = 0, a$ and $y = 0, b$ we would like to pose the following boundary conditions:

$$\text{At } x = 0, a: \qquad M_{xx} = M_{xy} = Q_x = 0. \tag{2.66}$$
$$\text{At } y = 0, b: \qquad M_{xy} = M_{yy} = Q_y = 0. \tag{2.67}$$

Unfortunately the system only admits two boundary conditions per edge. To overcome this discrepancy, the so-called generalized shear forces, combining boundary conditions from (2.66) and (2.67) are introduced. According to [6], p. 84, they are defined as

$$V_x = Q_x + \frac{\partial M_{xy}}{\partial y}, \tag{2.68}$$
$$V_y = Q_y + \frac{\partial M_{xy}}{\partial x}. \tag{2.69}$$

With this, the boundary conditions at a free boundary then become:

$$\text{At } x = 0, a: \qquad M_{xx} = V_x = 0. \tag{2.70}$$
$$\text{At } y = 0, b: \qquad M_{yy} = V_y = 0. \tag{2.71}$$

By substituting (2.28) and (2.29) into these boundary conditions, they become
At $x = 0, a$:

$$\frac{\partial^2 w}{\partial x^2} + \nu_{yx}\frac{\partial^2 w}{\partial y^2} = 0, \tag{2.72}$$
$$\frac{\partial^3 w}{\partial x^3} + \left(\nu_{yx} + \frac{4G_{xy}(1-\nu_{xy}\nu_{yx})}{E_x}\right)\frac{\partial^3 w}{\partial x \partial y^2} = 0. \tag{2.73}$$

And analogously at $y = 0, b$:

$$\nu_{xy}\frac{\partial^2 w}{\partial x^2} + \frac{\partial^2 w}{\partial y^2} = 0, \tag{2.74}$$
$$\frac{\partial^3 w}{\partial y^3} + \left(\nu_{xy} + \frac{4G_{xy}(1-\nu_{xy}\nu_{yx})}{E_y}\right)\frac{\partial^3 w}{\partial x^2 \partial y} = 0. \tag{2.75}$$

We continue with making this formulation dimensionless, which makes it more appropriate for numerical calculations.

2.4.5 Normalization and nondimensionalization

With equations (2.52) and (2.63) we have a system of two coupled fourth-order partial differential equations describing the coupling between in-plane deformations and large out-of-plane deflections:

$$\frac{\partial^2 \varepsilon^h_{xx}}{\partial y^2} + \frac{\partial^2 \varepsilon^h_{yy}}{\partial x^2} + \frac{1}{E_y}\frac{\partial^4 \varphi}{\partial x^4} + \left(\frac{1}{G_{xy}} - 2\frac{\nu_{xy}}{E_x}\right)\frac{\partial^4 \varphi}{\partial x^2 \partial y^2} + \frac{1}{E_x}\frac{\partial^4 \varphi}{\partial y^4} = \left(\frac{\partial^2 w}{\partial x \partial y}\right)^2 - \frac{\partial^2 w}{\partial x^2}\frac{\partial^2 w}{\partial y^2}, \tag{2.76}$$

and

$$\frac{2h^3}{3}\left(\frac{E_x}{1-\nu_{xy}\nu_{yx}}\frac{\partial^4 w}{\partial x^4} + 2\left(\frac{\nu_{yx}E_x}{1-\nu_{xy}\nu_{yx}} + G_{xy}\right)\frac{\partial^4 w}{\partial x^2 \partial y^2} + \frac{E_y}{1-\nu_{xy}\nu_{yx}}\frac{\partial^4 w}{\partial y^4}\right)$$
$$= q(x,y) + 2h\left(\frac{\partial^2 \varphi}{\partial x^2}\frac{\partial^2 w}{\partial y^2} + \frac{\partial^2 \varphi}{\partial y^2}\frac{\partial^2 w}{\partial x^2} - 2\frac{\partial^2 \varphi}{\partial x \partial y}\frac{\partial^2 w}{\partial x \partial y}\right). \tag{2.77}$$

Let us introduce the following dimensionless variables:

$$\hat{w} := \frac{w}{W}, \quad \hat{\varphi} = \frac{\varphi}{\Phi}, \quad \hat{\varepsilon}^h_{xx} := \frac{\varepsilon^h_{xx}}{\varepsilon_0}, \quad \hat{\varepsilon}^h_{yy} := \frac{\varepsilon^h_{yy}}{\varepsilon_0}, \quad \hat{x} := \frac{x}{L}, \quad \hat{y} := \frac{y}{L}, \quad \hat{q} = \frac{q}{Q}, \quad \hat{a} = \frac{a}{L}, \quad \hat{b} = \frac{b}{L}, \tag{2.78}$$

where the yet unknown factors W, Φ, ε_0 and Q will be specified in the following dimensional analysis. We rewrite (2.76) using these variables into

$$\frac{\varepsilon_0}{L^2}\left(\frac{\partial^2 \hat{\varepsilon}^h_{xx}}{\partial \hat{y}^2} + \frac{\partial^2 \hat{\varepsilon}^h_{yy}}{\partial \hat{x}^2}\right) + \frac{\Phi}{E_x L^4}\left(\frac{\partial^4 \hat{\varphi}}{\partial \hat{y}^4} + \left(\frac{E_x}{G_{xy}} - 2\nu_{xy}\right)\frac{\partial^4 \hat{\varphi}}{\partial \hat{x}^2 \partial \hat{y}^2} + \frac{E_x}{E_y}\frac{\partial^4 \hat{\varphi}}{\partial \hat{x}^4}\right) = \frac{W^2}{L^4}\left(\left(\frac{\partial^2 \hat{w}}{\partial \hat{x}\partial \hat{y}}\right)^2 - \frac{\partial^2 \hat{w}}{\partial \hat{x}^2}\frac{\partial^2 \hat{w}}{\partial \hat{y}^2}\right). \tag{2.79}$$

To make all terms of the same order of magnitude we take $\Phi = \varepsilon_0 E_x L^2, W = \sqrt{\varepsilon_0} L$, with ε_0 still free to choose. This reduces (2.79), after removing the hats, to

$$\frac{\partial^2 \varepsilon^h_{xx}}{\partial y^2} + \frac{\partial^2 \varepsilon^h_{yy}}{\partial x^2} + \frac{E_x}{E_y}\frac{\partial^4 \varphi}{\partial x^4} + \left(\frac{E_x}{G_{xy}} - 2\nu_{xy}\right)\frac{\partial^4 \varphi}{\partial x^2 \partial y^2} + \frac{\partial^4 \varphi}{\partial y^4} = \left(\frac{\partial^2 w}{\partial x \partial y}\right)^2 - \frac{\partial^2 w}{\partial x^2}\frac{\partial^2 w}{\partial y^2}. \tag{2.80}$$

Introducing the dimensionless variables together with the obtained results for Φ and W in (2.77), yields

$$\frac{2h^3 E_x}{3(1-\nu_{xy}\nu_{yx})}\frac{\sqrt{\varepsilon_0}}{L^3}\left(\frac{\partial^4 \hat{w}}{\partial \hat{x}^4} + 2\left(\nu_{yx} + \frac{(1-\nu_{xy}\nu_{yx})G_{xy}}{E_x}\right)\frac{\partial^4 \hat{w}}{\partial \hat{x}^2 \partial \hat{y}^2} + \frac{E_y}{E_x}\frac{\partial^4 \hat{w}}{\partial \hat{y}^4}\right) = Q\hat{q} + 2hE_x\frac{\varepsilon_0^{3/2}}{L}\left(\frac{\partial^2 \hat{\varphi}}{\partial \hat{x}^2}\frac{\partial^2 \hat{w}}{\partial \hat{y}^2} + \frac{\partial^2 \hat{\varphi}}{\partial \hat{y}^2}\frac{\partial^2 \hat{w}}{\partial \hat{x}^2} - 2\frac{\partial^2 \hat{\varphi}}{\partial \hat{x}\partial \hat{y}}\frac{\partial^2 \hat{w}}{\partial \hat{x}\partial \hat{y}}\right). \tag{2.81}$$

To make the terms of the same magnitude we take

$$Q = \frac{2h^3 E_x}{3(1-\nu_{xy}\nu_{yx})}\frac{\sqrt{\varepsilon_0}}{L^3}. \tag{2.82}$$

We divide (2.81) by Q and remove the hat to obtain the dimensionless equation

$$\frac{\partial^4 w}{\partial x^4} + 2\left(\nu_{yx} + \frac{(1-\nu_{xy}\nu_{yx})G_{xy}}{E_x}\right)\frac{\partial^4 w}{\partial x^2 \partial y^2} + \frac{E_y}{E_x}\frac{\partial^4 w}{\partial y^4} = q + \mu\left(\frac{\partial^2 \varphi}{\partial x^2}\frac{\partial^2 w}{\partial y^2} + \frac{\partial^2 \varphi}{\partial y^2}\frac{\partial^2 w}{\partial x^2} - 2\frac{\partial^2 \varphi}{\partial x \partial y}\frac{\partial^2 w}{\partial x \partial y}\right), \tag{2.83}$$

where $\mu = 3(1-\nu_{xy}\nu_{yx})\varepsilon_0(L/h)^2$, a dimensionless number. Thus, we arrived at the final equations in nondimensional form:

$$\frac{\partial^2 \varepsilon^h_{xx}}{\partial y^2} + \frac{\partial^2 \varepsilon^h_{yy}}{\partial x^2} + \frac{E_x}{E_y}\frac{\partial^4 \varphi}{\partial x^4} + \left(\frac{E_x}{G_{xy}} - 2\nu_{xy}\right)\frac{\partial^4 \varphi}{\partial x^2 \partial y^2} + \frac{\partial^4 \varphi}{\partial y^4} = \left(\frac{\partial^2 w}{\partial x \partial y}\right)^2 - \frac{\partial^2 w}{\partial x^2}\frac{\partial^2 w}{\partial y^2}, \tag{2.84}$$

$$\frac{\partial^4 w}{\partial x^4} + 2\left(\nu_{yx} + \frac{(1-\nu_{xy}\nu_{yx})G_{xy}}{E_x}\right)\frac{\partial^4 w}{\partial x^2 \partial y^2} + \frac{E_y}{E_x}\frac{\partial^4 w}{\partial y^4} = q + \mu\left(\frac{\partial^2 \varphi}{\partial x^2}\frac{\partial^2 w}{\partial y^2} + \frac{\partial^2 \varphi}{\partial y^2}\frac{\partial^2 w}{\partial x^2} - 2\frac{\partial^2 \varphi}{\partial x \partial y}\frac{\partial^2 w}{\partial x \partial y}\right). \tag{2.85}$$

Here, only μ is still undetermined, since it depends on ε_0. Seeing that ε_0 is a scale for the in-plane stresses induced by the wetting of the sheet, we choose $\varepsilon_0 = \beta_x \chi$, yielding

$$\mu = 3(1-\nu_{xy}\nu_{yx})\beta_x \chi \frac{L^2}{h^2} \tag{2.86}$$

Since, according to the third assumption of the Kirchhoff hypothesis outlined in Section 2.2, the in-plane deformations are of $\mathcal{O}(\delta^2)$, meaning ε_0 is as well, the dimensionless number μ is of $\mathcal{O}(1)$, provided the length to thickness ratio of the plate is small.

2.5 Buckling theory

The von Kármán equations (2.84),(2.85) are nonlinear. Therefore, unicity of the solution to these equations is not guaranteed; there can, and will sometimes, be multiple solutions. For small moisture-induced loads, there will be only one solution, the so-called pre-buckling solution, in which the flat configuration of the plate is maintained. At a certain critical magnitude of the load, a bifurcation of the solution will occur [8]. For values beyond this critical load, also solutions with $w \neq 0$ will exist. The $w = 0$-state will become unstable, whereas the $w \neq 0$-states, the buckled states are stable now. We then say that the plate is buckled and the critical magnitude of the loads is called the buckling load, or buckling threshold. We take a closer look at the dimensionless generalized von Kármán equations (2.84), (2.85), without a vertical load ($q = 0$):

$$\frac{\partial^2 \varepsilon^h_{xx}}{\partial y^2} + \frac{\partial^2 \varepsilon^h_{yy}}{\partial x^2} + \frac{E_x}{E_y}\frac{\partial^4 \varphi}{\partial x^4} + \Big(\frac{E_x}{G_{xy}} - 2\nu_{xy}\Big)\frac{\partial^4 \varphi}{\partial x^2 \partial y^2} + \frac{\partial^4 \varphi}{\partial y^4} = \Big(\frac{\partial^2 w}{\partial x \partial y}\Big)^2 - \frac{\partial^2 w}{\partial x^2}\frac{\partial^2 w}{\partial y^2}, \tag{2.87}$$

$$\frac{\partial^4 w}{\partial x^4} + 2\Big(\nu_{yx} + \frac{(1 - \nu_{xy}\nu_{yx})G_{xy}}{E_x}\Big)\frac{\partial^4 w}{\partial x^2 \partial y^2} + \frac{E_y}{E_x}\frac{\partial^4 w}{\partial y^4} = \mu\left(\frac{\partial^2 \varphi}{\partial x^2}\frac{\partial^2 w}{\partial y^2} + \frac{\partial^2 \varphi}{\partial y^2}\frac{\partial^2 w}{\partial x^2} - 2\frac{\partial^2 \varphi}{\partial x \partial y}\frac{\partial^2 w}{\partial x \partial y}\right). \tag{2.88}$$

Without water-induced strains, i.e. $\varepsilon^h_{xx} = \varepsilon^h_{yy} = 0$, the system has a trivial equilibrium solution $\varphi = w = 0$, which corresponds to the initial state of the plate. The flat configuration of the plate, $w = 0$, remains a solution to (2.88), regardless of the water-induced strains. We expect that, for increasing moisture content χ at a region of the plate, the flat configuration is maintained, until a certain threshold value for the stresses in the plate is reached, at which the plate bends out of plane. In the case at hand, the threshold value for the stresses is reached resulting from a certain moisture content.

Finding complete solutions of the Von Kármán equations at values beyond the buckling load is a difficult task due to the structure of the equations. However, using the approach outlined below, approximating the buckling threshold and the deflection profile immediately after the onset of buckling can be done without the need to solve the complete system of equations.

- We assume a moisture profile to be given, having a characteristic order of magnitude.
- We solve (2.87) with $w = 0$ for φ with boundary conditions (2.64), (2.65).
- Using φ as determined before, we calculate w from (2.88), assuming the boundary conditions (2.72)-(2.75). We will find that this leads to an eigenvalue problem for μ. The smallest eigenvalue is the buckling threshold, the corresponding w is an approximation of the deflection shape immediately after buckling.

2.6 Variational formulation for a rectangular plate

An often used approach to solving the plate buckling problem is by considering the potential energy of the plate and the change thereof caused by a deflection. Often the Von Kármán equations are derived in this way. Most of the books cited in this thesis have a chapter devoted to variational methods, see for example [5], Chapter 7,[8], Chapter 6, and especially Washizu, [11], who dedicated a book to this topic. The potential energy for the situation under consideration consists of two parts: the strain energy due to bending, which accounts for the energy from the out-of-plane deformations of the plate, and the energy due to moisture-induced in-plane stresses, the sum of which will be minimized. The out-of-plane part strain energy for an orthotropic rectangular plate is obtained by multiplying the left-hand side of (2.88) with w and integrating this over the plate. After some partial integration we find

$$U = h\int_0^b \int_0^a \left(\Big(\frac{\partial^2 w}{\partial x^2}\Big)^2 + 2\nu_{yx}\frac{\partial^2 w}{\partial x^2}\frac{\partial^2 w}{\partial y^2} + \frac{E_y}{E_x}\left(\Big(\frac{\partial^2 w}{\partial y^2}\Big)^2 + \frac{4G_{xy}}{E_x}(1 - \nu_{xy}\nu_{yx})\Big(\frac{\partial^2 w}{\partial x \partial y}\Big)^2\right)\right) \mathrm{d}x\mathrm{d}y. \tag{2.89}$$

The energy due to hygrothermal stresses is found by applying the approach to the right-hand side of (2.88) and after some partial integration we find an expression in terms of first derivatives of w:

$$E_h = -2h\mu \int_0^b \int_0^a \left(\left(\frac{\partial w}{\partial x}\right)^2 \frac{\partial^2 \varphi}{\partial y^2} + \left(\frac{\partial w}{\partial y}\right)^2 \frac{\partial^2 \varphi}{\partial x^2} - 2\frac{\partial w}{\partial x}\frac{\partial w}{\partial y}\frac{\partial^2 \varphi}{\partial x \partial y} \right) \mathrm{d}x\mathrm{d}y. \tag{2.90}$$

The boundary terms drop out because of the boundary conditions for the stresses (2.64), (2.65). We apply the Rayleigh-Ritz method, [8], § 6.6, to the expression for the potential energy $\Pi = U - E_h$, the most important and difficult part of which is to choose a set of coordinate functions $g_m(x), h_n(y)$ to approximate w. These functions should span all the possible outcomes for w, but still be manageable in calculations. Furthermore, the restriction is placed upon them that they satisfy the kinematic boundary conditions, i.e. those concerning w and its first order derivatives. In this case, with free boundaries, there are no such boundary conditions. We take

$$w = \sum_{m=1}^{\infty} \sum_{n=1}^{\infty} W_{mn} g_m(x) h_n(y), \tag{2.91}$$

where we still have to specify $g_m(x)$ and $h_n(y)$, while the coefficients W_{mn} have to follow from the Rayleigh-Ritz method as shown in the following result (2.92). First we determine the stress function from (2.87) with $w = 0$. Next, we apply the Rayleigh-Ritz method of minimizing the energy functional, which consists of equating the derivatives of the potential energy Π with respect to the constants W_{mn} to zero. This way we find a stationary point of w, which is a necessary condition for a minimum. We substitute (2.91) into the expression for the potential energy $\Pi = U - E_h$, from (2.89),(2.90) and differentiate with respect to $W_{ij}, i, j \in 0, 1, \ldots$ to find:

$$\begin{aligned}
\frac{\partial \Pi}{\partial W_{ij}} &= 2h \sum_{m=1}^{M} \sum_{n=1}^{N} W_{mn} \\
&\int_0^b \int_0^a \Big(g_m''(x) g_i''(x) h_n(y) h_j(y) + \nu_{yx} \Big(g_m''(x) g_i(x) h_n(y) h_j''(y) + g_m(x) g_i''(x) h_n''(y) h_j(y) \Big) \\
&\qquad \frac{E_y}{E_x} g_m(x) g_i(x) h_n''(y) h_j''(y) + 2\frac{G_{xy}}{E_x}(1 - \nu_{xy}\nu_{yx}) g_m'(x) g_i'(x) h_n'(y) h_j'(y) \Big) \mathrm{d}x\mathrm{d}y \\
&+ 2h\mu \sum_{m=1}^{M} \sum_{n=1}^{N} W_{mn} \int_0^b \int_0^a \Big(g_i'(x) g_m'(x) h_j(y) h_n(y) \frac{\partial^2 \varphi}{\partial y^2} + g_i(x) g_m(x) h_j'(y) h_n'(y) \frac{\partial^2 \varphi}{\partial x^2} \\
&\qquad - \Big(g_i'(x) g_m(x) h_j(y) h_n'(y) + g_i(x) g_m'(x) h_j'(y) h_n(y) \Big) \frac{\partial^2 \varphi}{\partial x \partial y} \Big) \mathrm{d}x\mathrm{d}y = 0.
\end{aligned} \tag{2.92}$$

The leads to an eigenvalue problem in terms of μ. This method will be applied to the reference problem to be discussed in Chapter 4.

Chapter 3

Circular plates

In this chapter we consider the case of circular plates. We expand on an axissymmetric configuration of a circle wetted at its center, since this can be solved analytically up to and including the buckling threshold, without the use of variational methods. Therefore, this reference problem is suitable to explicitly showcase the influence of the parameters involved. We will first translate the von Kármán model into polar coordinates. Next we will solve this to find the stresses and eventually the buckling threshold and the first post-buckling mode.

3.1 The von Kármán model in polar coordinates

We consider a circular plate of thickness $2h$ subjected to a moisture content profile χ. The situation is considered to be axissymmetric, i.e. only dependent on the radius r and the height z, and not on the angle θ.
First we use the approach followed for the rectangular plate to derive the equations describing the deflection of the plate. Let u_r, u_θ and u_z denote the displacements in the $r-, \theta-$ and $z-$direction, respectively, and u and w the $r-$ and $z-$displacements, respectively, of the midplane, $z = 0$. This leads us to the following representation of the displacements:

$$u_r(r,z) = u(r) - zw'(r), \quad u_\theta(r,z) = 0, \quad u_z(r,z) = w(r). \tag{3.1}$$

We find the strain in the radial direction using (2.3) and (3.1) to be

$$\varepsilon_{rr} = \frac{du_r}{dr} = u'(r) + \frac{1}{2}(w'(r))^2 - zw''(r). \tag{3.2}$$

We derive the tangential component of the strain by considering that it depends on the radial displacement. If elements of an infinitesimal arc length $rd\theta$ move in the radial direction by u_r, the arc length grows to $(r + u_r)d\theta$. We obtain:

$$\varepsilon_{\theta\theta} = \frac{(r+u_r)d\theta - rd\theta}{rd\theta} = \frac{u_r}{r} = \frac{u(r)}{r} - \frac{z}{r}w'(r). \tag{3.3}$$

The component $\varepsilon_{r\theta}$ is zero because of axissymmetry. From (3.2) and (3.3) we obtain a compatibility equation:

$$\varepsilon_{rr} - \frac{d}{dr}\left(r\varepsilon_{\theta\theta}\right) = \frac{1}{2}(w'(r))^2. \tag{3.4}$$

The constitutive equations are in this case:

$$\begin{bmatrix} \varepsilon_{rr} \\ \varepsilon_{\theta\theta} \\ \varepsilon_{r\theta} \end{bmatrix} = \frac{1}{E}\begin{bmatrix} 1 & -\nu & 0 \\ -\nu & 1 & 0 \\ 0 & 0 & 1+\nu \end{bmatrix}\begin{bmatrix} \sigma_{rr} \\ \sigma_{\theta\theta} \\ \sigma_{r\theta} \end{bmatrix} + \beta\chi\begin{bmatrix} 1 \\ 1 \\ 0 \end{bmatrix}, \tag{3.5}$$

or inversely

$$\begin{bmatrix}\sigma_{rr}\\ \sigma_{\theta\theta}\\ \sigma_{r\theta}\end{bmatrix} = \frac{E}{1-\nu^2}\begin{bmatrix}1 & \nu & 0\\ \nu & 1 & 0\\ 0 & 0 & 1-\nu\end{bmatrix}\begin{bmatrix}\varepsilon_{rr}\\ \varepsilon_{\theta\theta}\\ \varepsilon_{r\theta}\end{bmatrix} - \frac{E\beta\chi}{1-2\nu}\begin{bmatrix}1\\ 1\\ 0\end{bmatrix}. \tag{3.6}$$

The in-plane force balance in the radial direction yields the equilibrium equation

$$\frac{1}{r}\left(\frac{d}{dr}(r\sigma_{rr}) - \sigma_{\theta\theta}\right) = \frac{d\sigma_{rr}}{dr} + \frac{\sigma_{rr}-\sigma_{\theta\theta}}{r} = 0. \tag{3.7}$$

We trivially comply by this equation by using a stress function $\psi(r)$:

$$\sigma_{rr} = \frac{\psi(r)}{r}, \quad \sigma_{\theta\theta} = \psi'(r). \tag{3.8}$$

We derive the in-plane large deflection equation in terms of this stress function from the compatibility equation (3.4), using (3.5):

$$\varepsilon_{rr} - \frac{d}{dr}(r\varepsilon_{\theta\theta}) = \frac{1}{E}\left(\sigma_{rr} - \nu\sigma_{\theta\theta} + E\beta\chi - \frac{d}{dr}\Big(r\big(\sigma_{\theta\theta} - \nu\sigma_{rr} + E\beta\chi\big)\Big)\right), \tag{3.9}$$

leading to

$$\psi''(r) + \frac{\psi'(r)}{r} - \frac{\psi(r)}{r^2} + E\beta\frac{d\chi}{dr} = -\frac{E}{2r}(w'(r))^2. \tag{3.10}$$

For the out-of-plane part we start with the result of Section 2.3, equation (2.45), without external forces:

$$t_{ij,j} + T^0_{jk}u_{i,jk} = 0. \tag{3.11}$$

Neglecting higher-order terms, we find for $i = r$ and $i = z$ two equilibrium equations:

$$\frac{\partial\sigma_{rr}}{\partial r} + \frac{\partial\sigma_{rz}}{\partial z} + \frac{\sigma_{rr}-\sigma_{\theta\theta}}{r} = 0, \tag{3.12}$$

$$\frac{\partial\sigma_{rz}}{\partial r} + \frac{1}{r}\sigma_{zr} + \frac{\partial\sigma_{zz}}{\partial z} + T^0_{rr}w''(r) + T^0_{\theta\theta}\frac{w'(r)}{r} = 0, \tag{3.13}$$

which become after integration

$$\frac{\partial M_{rr}}{\partial r} + \frac{1}{r}(M_{rr} - M_{\theta\theta}) - Q = 0, \tag{3.14}$$

$$\frac{\partial Q}{\partial r} + \frac{1}{r}Q + N^0_r w'' + N^0_\theta\frac{w'}{r} = 0, \tag{3.15}$$

with

$$M_{rr} = -D\left(w'' + \nu\frac{w'}{r}\right), \qquad M_{\theta\theta} = -D\left(\frac{w'}{r} + \nu w''\right), \tag{3.16}$$

$$N^0_r = 2hT^0_{rr} = 2h\frac{\psi}{r}, \qquad N^0_\theta = 2hT^0_{\theta\theta} = 2h\psi'. \tag{3.17}$$

Here, $D = 2Eh^3/(3(1-\nu^2))$ is known as the *flexural rigidity*. Eliminating the shear force Q from these equations we obtain:

$$D\Delta^2 w(r) = \frac{2h}{r}\Big(\psi(r)w''(r) + \psi'(r)w'(r)\Big), \tag{3.18}$$

with

$$\Delta = \frac{1}{r}\frac{d}{dr}\left(r\frac{d}{dr}\right). \tag{3.19}$$

3.2 Analytical solution method

3.2.1 Pre-buckling state

We consider a circular plate with radius R, of which an inner circle with radius a, located at the center, is uniformly moisturized. First we solve for ψ in the pre-buckling situation. We start using (3.10) with $w = 0$:

$$\psi''(r) + \frac{\psi'(r)}{r} - \frac{\psi(r)}{r^2} = 0, \tag{3.20}$$

with the boundary conditions:

- $\psi(r) < \infty$, especially in the center of the plate.
- u_r and σ_{rr} are continuous at the edge of the inner circle, $r = a$.
- $\sigma_{rr} = 0$, at $r = R$.

The general solution to (3.20) is

$$\psi(r) = \begin{cases} c_1 r + \dfrac{c_2}{r}, & 0 < r < a, \\ \\ \tilde{c_1} r + \dfrac{\tilde{c_2}}{r}, & a < r < R. \end{cases} \tag{3.21}$$

In the inner circle the first boundary condition puts a restriction on $\psi(r)$, leading to $c_2 = 0$. In the outer we apply the third boundary condition to find:

$$\sigma_{rr}(R) = \frac{\psi(R)}{R} = \tilde{c}_1 + \frac{\tilde{c}_2}{R^2} = 0, \tag{3.22}$$

leading to $\tilde{c}_2 = -\tilde{c}_1 R^2$ and

$$\psi(r) = \begin{cases} c_1 r, & 0 < r < a, \\ \\ \tilde{c}_1 \left(r - \dfrac{R^2}{r} \right), & a < r < R. \end{cases} \tag{3.23}$$

We equate c_1 and $\tilde{c}_1$ using the condition that σ_{rr} is continuous across $r = a$:

$$\sigma_{rr}(a) = \frac{\psi(a)}{a} = c_1 = \tilde{c}_1 \left(1 - \frac{R^2}{a^2} \right). \tag{3.24}$$

We substitute this representation of c_1 into (3.23):

$$\psi(r) = \begin{cases} \tilde{c}_1 \left(1 - \frac{R^2}{a^2} \right) r, & 0 < r < a, \\ \\ \tilde{c}_1 \left(r - \dfrac{R^2}{r} \right), & a < r < R. \end{cases} \tag{3.25}$$

We determine u_r in both areas. In $0 < r < a$ we find, using (3.5) and (3.2)

$$\sigma_{rr} = \frac{\psi(r)}{r} = \tilde{c}_1 \left(1 - \frac{R^2}{a^2} \right), \quad \sigma_{\theta\theta} = \psi'(r) = \tilde{c}_1 \left(1 - \frac{R^2}{a^2} \right), \tag{3.26}$$

$$\varepsilon_{rr} = \frac{1}{E}(\sigma_{rr} - \nu\sigma_{\theta\theta}) + \beta\chi = \frac{\tilde{c}_1}{E}(1 - \nu) \left(1 - \frac{R^2}{a^2} \right) + \beta\chi, \tag{3.27}$$

$$u_r = \left(\frac{\tilde{c}_1}{E}(1 - \nu) \left(1 - \frac{R^2}{a^2} \right) + \beta\chi \right) r. \tag{3.28}$$

On the other hand, in $a < r < R$ we obtain, again using (3.5) and (3.2),

$$\sigma_{rr} = \frac{\psi(r)}{r} = \tilde{c}_1\Big(1 - \frac{R^2}{r^2}\Big), \quad \sigma_{\theta\theta} = \psi'(r) = \tilde{c}_1\Big(1 + \frac{R^2}{r^2}\Big), \tag{3.29}$$

$$\varepsilon_{rr} = \frac{1}{E}(\sigma_{rr} - \nu\sigma_{\theta\theta}) = \frac{\tilde{c}_1}{E}\Big(1 - \frac{R^2}{r^2} - \nu - \nu\frac{R^2}{r^2}\Big), \tag{3.30}$$

$$u_r = \frac{\tilde{c}_1}{E}(1-\nu)r + (1+\nu)\frac{\tilde{c}_1 R^2}{E}\frac{1}{r}. \tag{3.31}$$

At $r = a$ these two representations for the displacement coincide, yielding

$$u_r = \left(\frac{\tilde{c}_1}{E}(1-\nu)\left(1 - \frac{R^2}{a^2}\right) + \beta\chi\right)a = \frac{\tilde{c}_1}{E}(1-\nu)a + (1+\nu)\frac{\tilde{c}_1 R^2}{E}\frac{1}{a}, \tag{3.32}$$

leading to

$$\tilde{c}_1 = \frac{a^2 E\beta\chi}{2R^2}, \tag{3.33}$$

and so

$$\psi(r) = \begin{cases} \dfrac{(a^2 - R^2)E\beta\chi}{2R^2}r, & 0 < r < a, \\[2ex] \dfrac{a^2 E\beta\chi}{2R^2}\left(r - \dfrac{R^2}{r}\right), & a < r < R. \end{cases} \tag{3.34}$$

3.2.2 Determination of the buckling threshold

Next we consider (3.18) with the stress function we just obtained:

$$D\Delta^2 w(r) = \frac{2h}{r}\Big(\psi(r)w''(r) + \psi'(r)w'(r)\Big), \tag{3.35}$$

to determine the minimal value of χ for which a non-zero solution for w exists. We rewrite this expression to

$$D\left(\left(\frac{d}{dr}\left(r\frac{d}{dr}\right)\right)^2 w(r)\right) = Dr\left(\frac{d^2}{dr^2} + \frac{1}{r}\frac{d}{dr}\right)\left(\frac{d^2}{dr^2} + \frac{1}{r}\frac{d}{dr}\right)w(r) = 2h\Big(\frac{d}{dr}(\psi(r)w'(r))\Big), \tag{3.36}$$

introduce $W(r) := w'(r)$ and integrate to obtain

$$W''(r) + \frac{W'(r)}{r} - \frac{W(r)}{r^2} = \frac{2h}{D}\frac{\psi(r)}{r}W(r). \tag{3.37}$$

First, for $0 < r < a$, we have

$$W_1''(r) + \frac{W_1'(r)}{r} - \frac{W_1(r)}{r^2} + \frac{h}{D}\frac{(R^2 - a^2)E\beta\chi}{R^2}W_1(r) = 0. \tag{3.38}$$

We introduce

$$A^2 := \frac{h}{D}(R^2 - a^2)E\beta\chi/R^2. \tag{3.39}$$

It is important to note that A is real-valued. We recognize Bessel's equation:

$$W_1''(r) + \frac{W_1'(r)}{r} - \frac{W_1(r)}{r^2} + A^2 W_1(r) = 0. \tag{3.40}$$

The solutions are superpositions of Bessel functions, see [10], Chapter 9:

$$W_1(r) = C_1 J_1(Ar) + \tilde{C}_1 Y_1(Ar). \tag{3.41}$$

Since W must be finite at the center of the circle, we find $\tilde{C}_1 = 0$.

For $a < r < R$ we have:

$$W_2''(r) + \frac{W_2'(r)}{r} + \left(B^2 - \frac{C^2}{r^2}\right) W_2(r) = 0, \tag{3.42}$$

with

$$B^2 := -\frac{ha^2 E\beta\chi}{DR^2}, \quad C^2 := 1 - \frac{ha^2 E\beta\chi}{D}. \tag{3.43}$$

To this the general solution is

$$W_2 = C_2 J_C(Br) + C_3 Y_C(Br). \tag{3.44}$$

This solution is also valid for complex values for B and C. The solution to (3.37) is now given by:

$$W(r) = \begin{cases} W_1(r), & 0 \le r < a \\ W_2(r), & a < r < R \end{cases} = \begin{cases} C_1 J_1(Ar), & 0 \le r < a, \\ C_2 J_C(Br) + C_3 Y_C(Br) & a < r < R. \end{cases} \tag{3.45}$$

with the boundary conditions:

- $W_1(a) = W_2(a)$.
- $M_{rr}(W_1(a)) = -D\left(W_1'(a) + \nu\frac{W_1(a)}{a}\right) = -D\left(W_2'(a) + \nu\frac{W_2(a)}{a}\right) = M_{rr}(W_2(a))$,
  leading to $W_1'(a) = W_2'(a)$.
- $M_{rr}(R) = -D\left(W_2'(R) + \nu\frac{W_2(R)}{R}\right) = 0$,
  leading to $W_2'(R) + \nu\frac{W_2(R)}{R} = 0$.

These conditions result in a homogeneous system of equations for the coefficient vector $\boldsymbol{C} = \{C_1, C_2, C_3\}$:

$$\mathcal{C}\boldsymbol{C} = 0, \tag{3.46}$$

with

$$\mathcal{C} = \begin{bmatrix} J_1(Aa) & -J_C(Ba) & -Y_C(Ba) \\ \frac{A}{2}\Big(J_0(Aa) - J_2(Aa)\Big) & -\frac{B}{2}\Big(J_{C-1}(Ba) - J_{C+1}(Ba)\Big) & -\frac{B}{2}\Big(Y_{C-1}(Ba) - Y_{C+1}(Ba)\Big) \\ 0 & \frac{B}{2}\Big(J_{C-1}(BR) - J_{C+1}(BR)\Big) + \frac{\nu}{R}J_C(BR) & \frac{B}{2}\Big(Y_{C-1}(BR) - Y_{C+1}(BR)\Big) + \frac{\nu}{R}Y_C(BR) \end{bmatrix}.$$

This system has a nontrivial solution if and only if the determinant of the matrix is zero. We are interested in the smallest value for χ for which a nontrivial solution exists, this smallest eigenvalue is the moisture content at which buckling occurs, which is what we are looking for. We solve this system using Wolfram Mathematica [16], the results are discussed in Chapter 6.

This page is intentionally left in its initial, undeformed, configuration.

Chapter 4

Analytical solution for rectangular plates

In this chapter we consider as a reference problem an orthotropic rectangular plate that is partially wetted. Firstly, the in-plane stress function of a plate which is exposed to a moisture content distribution is found. Next, the Rayleigh-Ritz method described at the end of Chapter 2 is applied to approximate the buckling threshold.

4.1 Solution for the stress function

We consider a rectangular plate with length a and width b, thickness $2h$. We introduce the coordinate system $(\xi, \eta, z) = (x/a, y/b, z)$ such that the plate occupies the space $\mathcal{G} = \{\xi, \eta, z |\ 0 \leq \xi \leq 1, 0 \leq \eta \leq 1, -h \leq z \leq h\}$. A region $\mathcal{G}_2$ is kept at its initial moisture content, while the remainder of the plate, $\mathcal{G}_1$, is exposed to a uniform rise in moisture content χ. We define $t(\xi, \eta) = I_{(\xi,\eta)\in\mathcal{G}_1}$, the identity function representing the wet region. We introduce the following dimensionless numbers:

$$E := \left(\frac{E_x}{E_y}\right)^{1/4}, \quad \gamma := \sqrt{\frac{E_x}{2G_{xy}} - \nu_{xy}}, \quad \beta := \frac{\beta_y}{\beta_x}. \tag{4.1}$$

We determine the stress function in both parts of the plate in the pre-buckling situation, using the von Kármán equations with $w = 0$:

$$E^4 \left(\frac{b}{a}\right)^2 \frac{\partial^4 \varphi}{\partial \xi^4} + 2\gamma^2 \frac{\partial^4 \varphi}{\partial \xi^2 \partial \eta^2} + \left(\frac{a}{b}\right)^2 \frac{\partial^4 \varphi}{\partial \eta^4} = -E_x ab\beta_x \chi \left(\frac{a}{b}\frac{\partial^2 t}{\partial \xi^2} + \frac{b}{a}\beta \frac{\partial^2 t}{\partial \eta^2}\right). \tag{4.2}$$

We note that the derivatives of t are infinite at the discontinuities, but since we will use the variational formulation of (4.2) in the following, we will obtain the relevant terms through partial integration.

For φ we choose the following form:

$$\varphi(\xi, \eta) = \sum_{m=1}^{M} \sum_{n=1}^{N} A_{mn} f_m(\xi) f_n(\eta), \tag{4.3}$$

with

$$f_i(x) = \cosh(\lambda_i x) - \cos(\lambda_i x) - \frac{\cosh(\lambda_i) - \cos(\lambda_i)}{\sinh(\lambda_i) - \sin(\lambda_i)} \Big(\sinh(\lambda_i x) - \sin(\lambda_i x)\Big). \tag{4.4}$$

These are the modes for a beam clamped at both edges [12]. For odd-numbered i these functions are symmetric around $x = 1/2$, for even values of i they are antisymmetric. The functions satisfy $f_i(0) = f_i(1) = f_i'(0) = 0$, while $f_i'(1)$ leads to the characteristic equation:

$$\sinh(\lambda_i) + \sin(\lambda_i) - \frac{\cosh(\lambda_i) - \cos(\lambda_i)}{\sinh(\lambda_i) - \sin(\lambda_i)} \left(\cosh(\lambda_i) - \cos(\lambda_i)\right) = 0. \tag{4.5}$$

Using these functions the boundary conditions for the stress are automatically satisfied:

$$\xi = 0, a, \quad f_i(0) = f_i(1) = 0, \quad \Rightarrow \quad \sigma_{xx} = \frac{\partial^2 \varphi}{\partial y^2} = 0 \tag{4.6}$$

$$f_i'(0) = f_i'(1) = 0 \quad \Rightarrow \quad \sigma_{xy} = \frac{\partial^2 \varphi}{\partial x \partial y} = 0, \tag{4.7}$$

and analogously for $\eta = 0, 1$, where $\sigma_{xy} = \sigma_{yy} = 0$.

To avoid numerical problems for larger values of i, we rewrite (4.4) to

$$f_i(x) = e^{-\lambda_i x} - \cos(\lambda_i x) - \delta_i \sinh(\lambda_i x) + \sigma_i \sin(\lambda_i x), \tag{4.8}$$

with

$$\delta_i = 2\, \frac{e^{-2\lambda_i} + (\sin(\lambda_i) - \cos(\lambda_i))e^{-\lambda_i}}{1 - e^{-2\lambda_i} - 2e^{-\lambda_i} \sin(\lambda_i)}, \qquad \sigma_i = \frac{\cosh(\lambda_i) - \cos(\lambda_i)}{\sinh(\lambda_i) - \sin(\lambda_i)}. \tag{4.9}$$

To find the values of (A_{mn}) we use a set of linear equations obtained by multiplying (4.2) with $f_r(\xi) f_s(\eta)$, for $r = 1, 2, \ldots, s = 1, 2, \ldots$ and integrate over the surface of the plate. Keeping in mind the orthogonality of (f_i) this process yields:

$$[\boldsymbol{C}]\,\{\boldsymbol{A}_{mn}\} = -E_x ab\beta_x \chi \{\mathbf{RHS}\}. \tag{4.10}$$

Here, $\boldsymbol{C}$ is of order $(MN \times MN)$. Its elements are given by

$$C_{mn,mn} = 2\gamma^2 \int_0^1 f_m''(\xi) f_m(\xi) \mathrm{d}\xi \int_0^1 f_n''(\eta) f_n(\eta) \mathrm{d}\eta \tag{4.11}$$

$$+ \lambda_m^4 E^4 \left(\frac{b}{a}\right)^2 \int_0^1 f_m^2(\xi) \mathrm{d}\xi \int_0^1 f_n^2(\eta) \mathrm{d}\eta + \lambda_n^4 \left(\frac{a}{b}\right)^2 \int_0^1 f_m^2(\xi) \mathrm{d}\xi \int_0^1 f_n^2(\eta) \mathrm{d}\eta \tag{4.12}$$

$$= 2\gamma^2 \int_0^1 \left(f_m'(\xi)\right)^2 \mathrm{d}\xi \int_0^1 \left(f_n'(\eta)\right)^2 \mathrm{d}\eta + \lambda_m^4 E^4 \left(\frac{b}{a}\right)^2 + \lambda_n^4 \left(\frac{a}{b}\right)^2. \tag{4.13}$$

for diagonal elements. The last expression is obtained by partial integration and by considering that $\int_0^1 f_k^2(x) \mathrm{d}x = 1, \forall k$. The elements of $\boldsymbol{C}$ are given by

$$C_{rs,mn} = 2\gamma^2 \int_0^1 f_r'(\xi) f_m'(\xi) \mathrm{d}\xi \int_0^1 f_s'(\eta) f_n'(\eta) \mathrm{d}\eta. \tag{4.14}$$

for off-diagonal terms. The $(mn)^{\text{th}}$ element of the right-hand side is given by:

$$-E_x ab\beta_x \chi \int_0^1 \int_0^1 \left(\frac{b}{a} f_m''(\xi) f_n(\eta) + \beta \frac{a}{b} f_m(\xi) f_n''(\eta)\right) t(\xi, \eta) \mathrm{d}\xi \mathrm{d}\eta. \tag{4.15}$$

Upon solving (4.10) we obtain $\{\boldsymbol{A_{mn}}\}$ and, using (4.3), $\varphi(\xi, \eta)$.

4.2 Application of the Rayleigh-Ritz method

Next we apply the variational formulation from Section 2.6 to the second Von Kármán equation to obtain an approximation of the buckling threshold. For w we choose the representation (compare with (2.91), but notice that we choose the same functions for $g_m(\xi)$ and $h_n(\eta)$ here)

$$w(\xi,\eta) = \sum_{i=1}^{I}\sum_{j=1}^{J} W_{ij} g_i(\xi) g_j(\eta). \tag{4.16}$$

In the cases considered in the following, we will assume a doubly symmetric moisture distribution, therefore we choose $(g_k(\xi))$ as symmetric about the center at $\xi,\eta = 1/2$. Furthermore, the functions need to be linearly independent. The options $g_k(\xi) = \cos(k/2\pi(\xi - \frac{1}{2}))$ and $g_k(\xi) = (\xi - \frac{1}{2})^{2k}$ are used in the following. The out-of-plane part of the strain energy is given by (2.89) as:

$$U = \frac{h^3}{3(1-\nu_{xy}\nu_{yx})ab}\int_0^1\int_0^1 \left(E_x \left(\frac{b}{a}\right)^2 \left(\frac{\partial^2 w}{\partial \xi^2}\right)^2 + 2E_x\nu_{yx}\frac{\partial^2 w}{\partial \xi^2}\frac{\partial^2 w}{\partial \eta^2} \right.$$
$$\left. + E_y \left(\frac{a}{b}\right)^2 \left(\frac{\partial^2 w}{\partial \eta^2}\right)^2 + 2G_{xy}(1-\nu_{xy}\nu_{yx}) \left(\frac{\partial^2 w}{\partial \xi \partial \eta}\right)^2 \right) \mathrm{d}\xi\mathrm{d}\eta.$$

We use (4.16) and differentiate with respect to W_{mn}; as in (2.92) this yields, with (x,y) replaced with (ξ,η),

$$\frac{\partial U}{\partial W_{mn}} = \frac{2h^3}{3(1-\nu_{xy}\nu_{yx})ab}\sum_{i=1}^{I}\sum_{j=1}^{J} W_{ij}$$
$$\int_0^1\int_0^1 \left(E_x \left(\frac{b}{a}\right)^2 g_m''(\xi) g_i''(\xi) g_n(\eta) g_j(\eta) + E_x\nu_{yx}\left(g_m''(\xi) g_i(\xi) g_n(\eta) g_j''(\eta) + g_m(\xi) g_i''(\xi) g_n''(\eta) g_j(\eta) \right) \right.$$
$$\left. + E_y \left(\frac{a}{b}\right)^2 g_m(\xi) g_i(\xi) g_n''(\eta) g_j''(\eta) + 2G_{xy}(1-\nu_{xy}\nu_{yx}) g_m'(\xi) g_i'(\xi) g_n'(\eta) g_j'(\eta) \right) \mathrm{d}\xi\mathrm{d}\eta.$$

The work done by in-plane stresses is, according to (2.90), here equal to:

$$E_h = h\int_0^1\int_0^1 \left(\frac{b}{a}\frac{\partial^2\varphi}{\partial\eta^2}\left(\frac{\partial w}{\partial \xi}\right)^2 + \frac{a}{b}\frac{\partial^2\varphi}{\partial\xi^2}\left(\frac{\partial w}{\partial \eta}\right)^2 - 2\frac{\partial^2\varphi}{\partial\xi\partial\eta}\frac{\partial w}{\partial\xi}\frac{\partial w}{\partial\eta} \right) \mathrm{d}\xi\mathrm{d}\eta. \tag{4.17}$$

Using (4.16) and differentiating with respect to W_{kl} we find:

$$\frac{\partial U_\sigma}{\partial W_{kl}} = 2h\sum_{i=1}^{I}\sum_{j=1}^{J} W_{ij}\int_0^1\int_0^1 \left(\frac{b}{a} g_i'(\xi) g_k'(\xi) g_j(\eta) g_l(\eta)\frac{\partial^2\varphi}{\partial\eta^2} + \frac{a}{b} g_i(\xi) g_k(\xi) g_j'(\eta) g_l'(\eta)\frac{\partial^2\varphi}{\partial\xi^2} \right.$$
$$\left. - \left(g_i'(\xi) g_k(\xi) g_j(\eta) g_l'(\eta) + g_i(\xi) g_k'(\xi) g_j'(\eta) g_l(\eta) \right)\frac{\partial^2\varphi}{\partial\xi\partial\eta} \right) \mathrm{d}\xi\mathrm{d}\eta.$$

Using (4.3) we rewrite this to

$$\frac{\partial U_T}{\partial W_{kl}} = -2hE_x\beta_x\chi\sum_{i=1}^{I}\sum_{j=1}^{J}\sum_{m=1}^{M}\sum_{n=1}^{N} W_{ij} A_{mn} \left(I_1 - I_2 - I_3 + I_4\right),$$

with

$$I_1 = \int_0^1 \int_0^1 \Big(f_m(\xi) g_i'(\xi) g_k'(\xi) f_n''(\eta) g_j(\eta) g_l(\eta) \Big) \mathrm{d}\xi \mathrm{d}\eta,$$
$$I_2 = \int_0^1 \int_0^1 \Big(f_m'(\xi) g_i'(\xi) g_k(\xi) f_n'(\eta) g_j(\eta) g_l'(\eta) \Big) \mathrm{d}\xi \mathrm{d}\eta,$$
$$I_3 = \int_0^1 \int_0^1 \Big(f_m'(\xi) g_i(\xi) g_k'(\xi) f_n'(\eta) g_j'(\eta) g_l(\eta) \Big) \mathrm{d}\xi \mathrm{d}\eta,$$
$$I_4 = \int_0^1 \int_0^1 \Big(f_m''(\xi) g_i(\xi) g_k(\xi) f_n(\eta) g_j'(\eta) g_l'(\eta) \Big) \mathrm{d}\xi \mathrm{d}\eta.$$

We solve the eigensystem

$$\left[\frac{\partial U}{\partial W_{kl}} - \tilde{\mu} \frac{\partial U_T}{\partial W_{kl}} \right] \{W_{ij}\} = 0, \tag{4.18}$$

with

$$\tilde{\mu} = E_x \beta_x \chi_0, \tag{4.19}$$

to find $\tilde{\mu}$ and thereby the buckling threshold χ_0. The results of this procedure will be discussed in Chapter 6.

Chapter 5

Numerical approach

Parallel to the analytical solution approach we will also consider a simulation. A simulation can be more easily extended to better reflect reality in ways that are hard to analyze with von Kármán theory. The simulation will be compared with the analytical model in the next chapter.

The simulation is carried out using Marc Mentat [14]. This is a commercially available finite element software package, especially equipped to deal with nonlinear problems. Marc Mentat receives input from a text file, referred to as a procedure, containing all information necessary to set up the simulation, such as nodal coordinates and numerical preferences. This file is generated using MATLAB [15] since this makes it easier to change parameters like the number of elements and still keep the file valid. The setup of the simulation roughly consists of the following steps:

- Defining a grid.
- Entering material properties.
- Applying initial conditions and boundary conditions.
- Setting numerical preferences.

Each of the steps will be discussed in more detail.

The grid is defined by creating a circle or a rectangle for the problems considered in Chapter 3 and 4, respectively, and subdividing it uniformly. The rectangular plate is subdivided into rectangles by partitioning it uniformly. For the circle polar coordinates are used. The radius and the angle are subdivided and edges of elements are linearized. This means that near the center triangular elements are created. Caution should be taken when handling these. We will look at this in more detail when discussing the boundary conditions. Away from the center trapezoidally shaped elements will be created. This means that the plate is not exactly circular. So to represent the shape of the plate and the wetted circular region the angle has to be subdivided into many parts. In the wetted region a finer grid will be used to better capture the stress distribution.

Like the analytical model, the simulation is two-dimensional. This is achieved by use of using shell elements. The thickness is a design variable for the elements. Element number 75 [18] is used, which is described as being a bilinear thick-shell element. The thick-shell property of this element signifies that it is based on Von Kármán theory, which makes it suitable for this simulation. Marc Mentat also provides a quadratic thick-shell element, but it is computationally more expensive and tests have shown that it does not provide results differing from those obtained using the bilinear element. The shell element provides an option to set a number of integration points in the thickness direction. The default option for this design variable is 11. Tests have shown that varying this odd-numbered parameter between 1 and 21 does not impact the results. This is to be expected since we do not vary any parameters in the thickness direction. If, for example, a moisture distribution which varies in the thickness direction is used, this design variable will probably come into play.

Next, we define the material as elastic and enter the parameters appearing in Hooke's law (2.21): Young's moduli, Poisson ratios, shear moduli and coefficients of hygroexpansivity. Also, the density of the material needs to be given. This parameter does not appear in the von Kármán model described before, since we consider a static problem, but it is relevant for the simulation when forces are applied to the plate.

The boundary conditions at the edges of the plate are not explicitly imposed. By not imposing boundary conditions, the free edge boundary conditions (2.64), (2.65) are satisfied. This is reflected in the simulation results, as we will discuss in the next chapter. We do need to impose conditions to prevent rigid-body movement. For the circular plate described in Chapter 3 we fix the center. However, if we fix only the central node we encounter numerical errors. This is probably due to the triangular elements near the center or due to singularities. To resolve this issue we fix the central node and the nodes adjacent to it. The three displacements and the three rotations are set at 0 for these nodes during the entire simulation. For the rectangular plate we also fix the node at the center and the nodes adjacent to it.

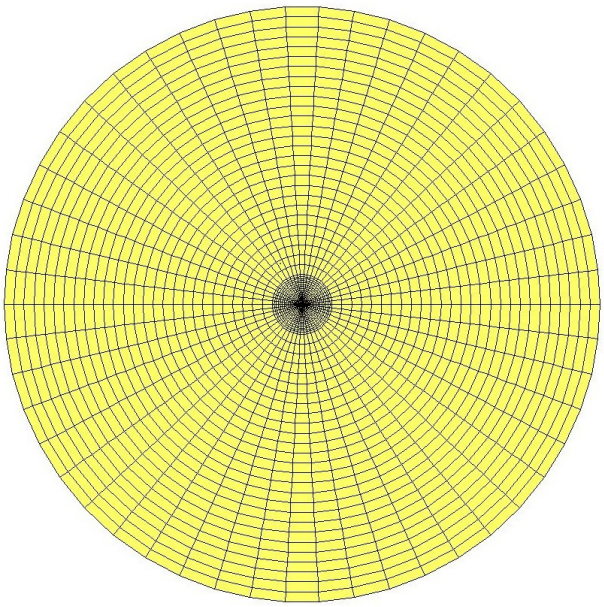

Figure 5.1: The grid used for the simulation, with 30 subdivisions in the radial direction and 50 in the tangential division. Each of the elements in the wetted central circle are subdivided into 5 elements.

Since $w = 0$ remains a solution to the Von Kármán equations, even after the buckling threshold has been reached, running the simulation as it is would not result in the buckling of the plate. To induce displacement in the z-direction we need to apply some sort of imperfection, to push the plate out of its initial position once the moisture content is high enough. This can be done in multiple ways:

- Applying a small imperfection force to the plate at the start of the simulation.
- Imposing a small difference in moisture content between the lower and upper side of the plate.
- Randomizing the z-coordinates of the initial position of the nodes to vary slightly from the reference position.

Because of good initial results, the first of the options was chosen for the circular problem. The simulation results have not given a reason to change this since. Care must be taken where to apply the force and what magnitude it should have. The results of the simulation must be independent of the exact magnitude of the forces applied. In the case of the circle we need to preserve the axissymmetry, so we apply the same force to all nodes outside of the wetted region. This way no net moment is imposed. The magnitude of the force has to be determined by trial and error and depends heavily on the parameter values. For the rectangular plate the randomization of the initial position provides better results. Tries with an imperfection proved it be impractical since the range in which the magnitude of the forces must fall in is small. This means that many simulations have to be executed to find a good magnitude by trial and error. Applying an imperfection which is too small will not result in buckling, however too large an imperfection will result in a lengthy calculation causing divergence, or a severe deformation of the plate before the buckling threshold is reached, distorting the results.

There is no option in Marc Mentat to simulate hygroexpansion of the plate. Therefore we will raise the temperature in the simulation. As discussed in Section 2.2, this is modeled in the same way. According to the user manual [17] the thermo-mechanical analysis Marc Mentat performs uses the same formulation

we do. We just have to set the coefficient of thermal expansion used in the simulation to the value of the hygro-expansivity coefficient β. For consistency, we will keep referring to wetting of paper in the following instead of heating.

During the simulation the moisture content will be raised in steps, which in Marc jargon is referred to as virtual time steps. This does not mean that we solve a dynamic problem, no inertia or vibration characteristics are taken into account. It does include damping characteristics to improve convergence of the nonlinear calculations. It is not clear from the documentation how exactly this is implemented. At every time step the system is solved, using the solution of the previous steps. This step-wise calculation is necessary to capture the instance of buckling, without it the simulation will skip over it and keep the plate in its initial position. The step size should be chosen small enough not to skip over the buckling threshold and to accurately determine it. This is computationally expensive however. Marc uses an algorithm that halves the step size when the solution method does not converge in a step. Usually this causes the step to be reduced near the onset of buckling, since the simulation exhibits highly nonlinear behavior there.

Because we are dealing with a nonlinear situation, the numerical method should be chosen accordingly. Here, the full Newton-Raphson method is used. For the Newton-Raphson iteration, Marc allows the option to define a convergence criterion. The options for this are residual force, displacement and strain energy. Residual force refers to the virtual force the simulation has to add to the system to keep the plate in equilibrium. The standard option is a relative residual force tolerance of 0.1, which is grossly insufficient and should only be used to test a simulation setup. For the instances that the simulation has been used for this report, this is lowered to 0.0001, which appears to give good results, and keeps the computation time at an acceptable level.

To get results for successive values of the moisture content, time integration with a direct integration method is used, using the single step Houbolt operator. It has strong damping characteristics, making it especially suitable for highly nonlinear calculations such as this one. In addition, it is unconditionally stable and second order accurate. This operator is based on a cubic polynomial fit through three previous points in time (moisture content) and is given by [17], chapter 5:

$$\left(\frac{2}{\Delta t^2}M + \frac{11}{6\Delta t}C + K\right)\Delta u = F^{n+1} - R^n + \frac{1}{\Delta t^2}\left(3u^n - 4u^{n-1} + u^{n-2}\right)M + \frac{1}{\Delta t}\left(\frac{7}{6}u^n - \frac{3}{2}u^{n-1} + \frac{1}{3}u^{n-2}\right)C. \tag{5.1}$$

With M, C and K the mass, damping and stiffness matrix respectively, F the external forces, R the internal forces, and u the displacements. Superscript n's denote subsequent time (moisture content) steps and ΔT the time (moisture content) step size. Since we perform a static analysis, the mass matrix M is taken out of the formulation. Marc/Mentat does not provide documentation on how these matrices are formed and there is no option in the program to show them. This is probably information MSC. software chooses not to publish because of commercial considerations. The algorithm used by Marc has a way of dealing with subsequent time (moisture content) steps that vary in size, but the way this is done is not published.

Both the Newton-Raphson method and the single step Houbolt operator are recommended by the Marc user manual [17], Chapter 11, for nonlinear problems and are widely used. Initial testing with other numerical methods and the behavior of the simulations done to obtain the results displayed in this report give no indication that the other methods provided in Marc/Mentat will provide better results.

The aspects mentioned above are just a small fraction of the possible options Marc/Mentat provides. For most of these, the option chosen is either the default option, or the choice recommended by the user manual for these kind of simulations.

This page is intentionally left in its initial, undeformed, configuration.

Chapter 6

Results and discussion

The results of the simulation and the analytical solution for the reference problem of the circular plate problem from Chapter 3 will be discussed here. We will compare the stresses and displacements in the pre-buckling moisture content range. Next we will determine the buckling threshold for values close to the values paper would realistically have, to obtain a comparison between the simulation and the analytical method. Also we will research the influence of the parameters on the value of the buckling threshold.

Next we will consider the rectangular plate. We will compare the stresses and displacements in the pre-buckling moisture content range. Then we will compare the buckling threshold obtained through simulation with the value obtained by means of the Rayleigh-Ritz method for four plates with various parameter values.

6.1 Circular plate

To compare various results from the two approaches for the circular plate, we will initially use the following values for the relevant parameters:

- $R = 1\text{m}$
- $a = 0.1\text{m}$
- $E = 5 \cdot 10^9\text{Pa}$
- $\nu = 0.3$
- $h = 0.01\text{m}$ (the thickness of the plate is $2h = 0.02\text{m}$)
- $\beta = 0.001$
- $\chi = 1\%$

For these simulations an initial 1500 elements grid will be used, the radial and tangential curves are subdivided into 30 and 50 curves respectively. Then, each element in the wetted part is subdivided into 3 elements in the radial direction, increasing the total number of elements to 1800. The initial time (moisture content) step size is taken to be $1/200^{\text{th}}$ of the simulation length. As mentioned in the previous chapter, the algorithm MARC uses varies this time step size during the simulation. For these parameter values, the Airy stress function, and the two stress components, given by (3.8) and (3.34) are shown in Figure 6.1. We note that the radial stress is indeed continuous and it vanishes at the edge at $r = 1$, as demanded by the boundary conditions. For comparison, the radial and tangential stresses resulting from the simulation for the same parameter values are given in Figure 6.2. Apart from the difference near the center of the plate at $r = 0$, these results are similar to those obtained analytically. The discrepancy is likely caused by the boundary conditions imposed at the center, needed to prevent rigid body movements in the simulation.

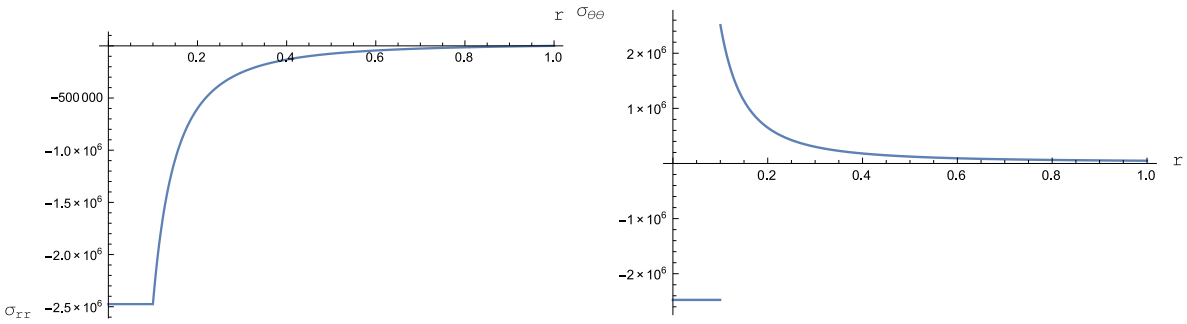

(a) Radial stress, $\sigma_{rr}(r)$.

(b) Tangential stress, $\sigma_{\theta\theta}(r)$.

Figure 6.1: The stress components obtained obtained from the analytical method, for the parameter values given in the text.

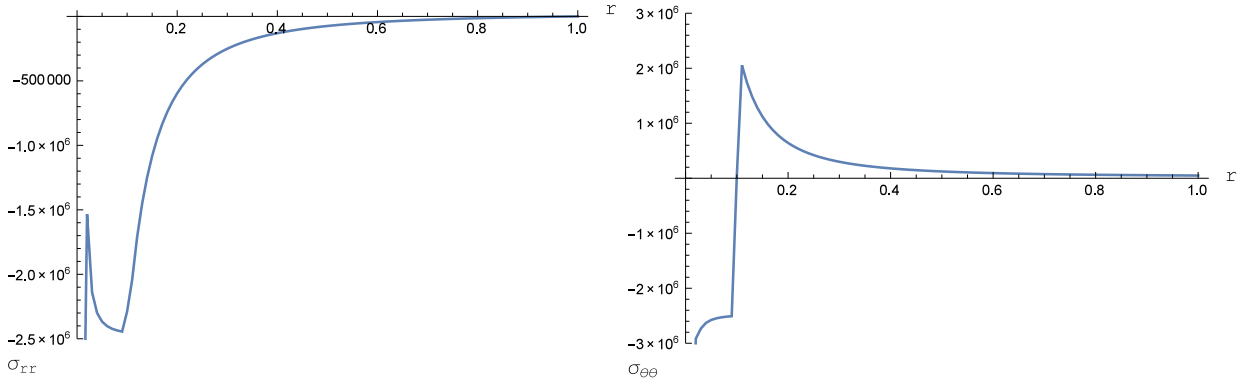

(a) Radial stress, $\sigma_{rr}(r)$.

(b) Tangential stress, $\sigma_{\theta\theta}(r)$.

Figure 6.2: The stress components as given by the simulation, for the same parameter values.

The displacement in the radial direction is given by (3.32). The comparison between the analytical solution and the simulation results for this quantity is shown in Figure 6.3. A good agreement is shown, also the boundary condition of continuity over $r = a$ is satisfied.

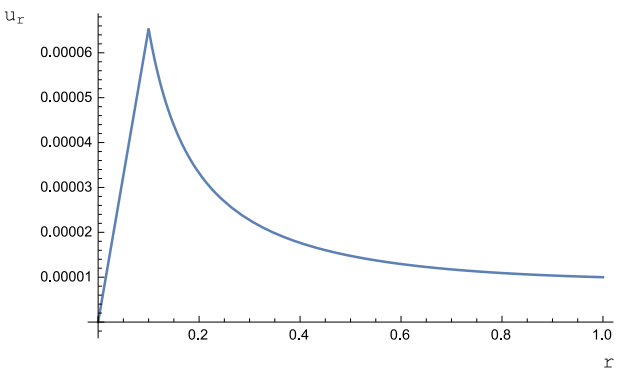

(a) Radial displacement, $u_r(r)$, analytical solution.

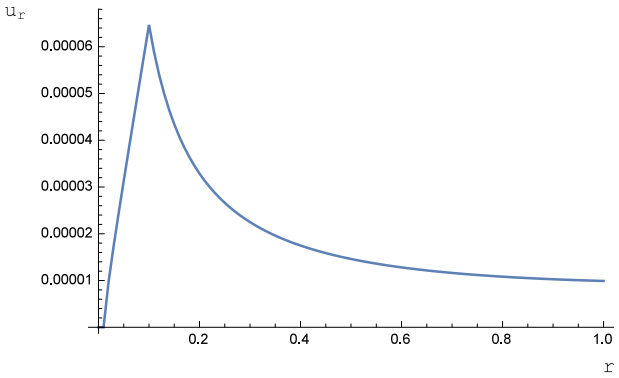

(b) Radial displacement, $u_r(r)$, simulation.

Figure 6.3: The displacement in radial direction, results from the analytical solution and the simulation.

6.1.1 Parameters determining the buckling threshold

Now that we have briefly verified that the simulation provides results similar to the analytical results for the circular plate reference problem in the pre-buckling situation, we move on to the onset of buckling. As an illustrative example, the vertical displacement of a node at the edge of the plate resulting from the simulation is shown in Figure 6.4. This is done with $E = 5 \cdot 10^9, \nu = 0.3, R = 1, a = 0.1$. We clearly see that the buckling threshold is reached at approximately $0.58 - 0.59$ times the simulation length. The drastic change in z-displacement makes this figure suitable to manually determine the buckling threshold. We introduce the symbol χ_0 to indicate the moisture content at which buckling occurs.

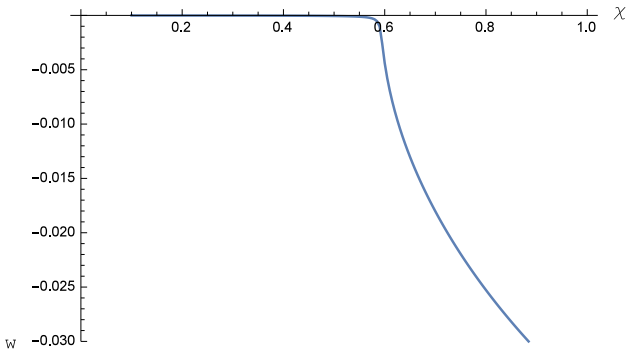

Figure 6.4: Simulation results for the vertical displacement of a node along the edge. On the x-axis we see the virtual time. The parameter values given in the previous section, with the exception of the (scaled) moisture content χ, have been used.

In Figure 6.5 we show the shape the plate attains after buckling, obtained through simulation. As expected, it maintains its axissymmetry in the simulation. The shape of the plate immediately after buckling can be determined from the analytical solution, however the magnitude of the deflection cannot because of the nonlinear character of the equations. This allows us to compare the FEM solution to the analytical work on the shape of the plate immediately after buckling. A good agreement is shown in Figure 6.6. Varying the relevant parameters individually from the previously used values should give us a first glance at the influence of each of them on the buckling threshold. The influence of β is quite obvious because of its definition; the critical value of the moisture content χ_0 is inversely proportional to this parameter. Looking at the structure of the system (3.46), we see that χ_0 only depends on h, β and E through A, B and C. Substituting the flexural rigidity $D = 2Eh^3/(3(1-\nu^2))$ into the expressions for A, B, C, (3.39) and (3.43) we find:

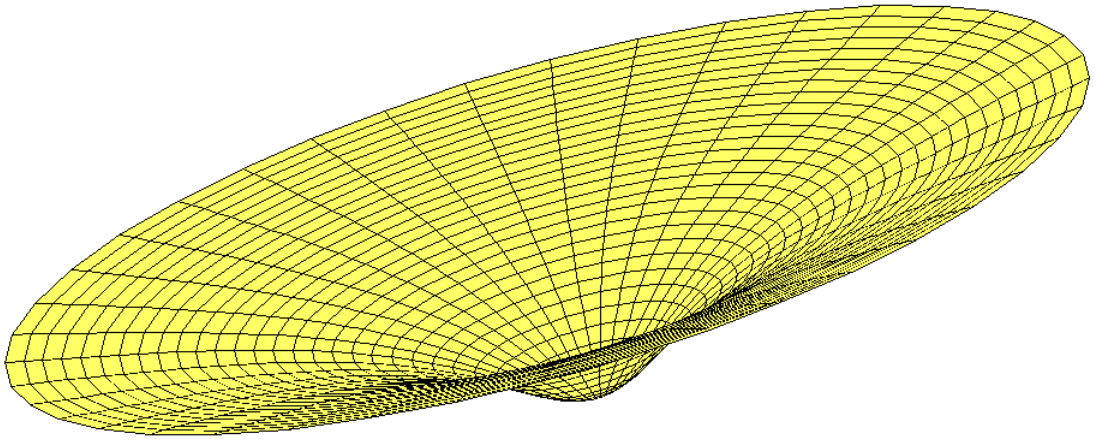

Figure 6.5: The shape of the circular plate after buckling, simulation result.

$$
\begin{aligned}
A^2 &= \frac{R^2 - a^2}{R^2} \frac{3(1-\nu^2)}{2h^2} \beta\chi, \\
B^2 &= \frac{a^2}{R^2} \frac{3(1-\nu^2)}{2h^2} \beta\chi, \\
C^2 &= 1 - a^2 \frac{3(1-\nu^2)}{2h^2} \beta\chi.
\end{aligned}
\tag{6.1}
$$

We note that these expressions are independent of E and conclude that the plate's Young's modulus has no influence on the buckling threshold χ_0. Physically this means that the out-of-plane strain energy and the hygrothermal energy depend on E in the same way: linearly.

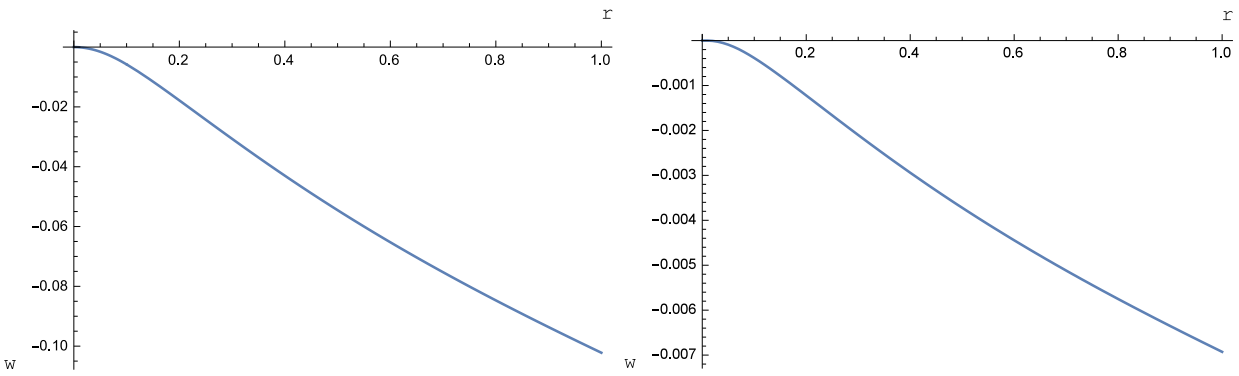

(a) Vertical displacement of the plate, analytical solution.

(b) Vertical displacement of the plate, simulation.

Figure 6.6: Comparison of the two methods in determining the shape of the plate immediately after buckling. On the horizontal axis r is varied between the center and the edge of plate. We should disregard the values on the vertical axis, since the analytical solution does not provide the magnitude of the displacement.

Also we see a quadratic relationship between h and χ_0 in all three of the equations. Finally, we note that, since the plate's Poisson ratio ν has a value between 0.2 and 0.4 for paper, a change in it will not change A, B and C by much, since it appears as $(1-\nu^2)$ in the equations. The effect of varying the relevant parameters from the values given in the previous section is shown in Figure 6.7. From physical considerations, we would

expect that a plate that is not wetted ($a = 0$) or completely wetted ($a = R$) will not buckle however high we set the moisture content. These instances appear in the graphs as asymptotes. We see that the buckling threshold converges to a certain limit as $R \to \infty$. This indicates that for large values of R the effects of increasing R/a and of increasing R/h cancel each other out.

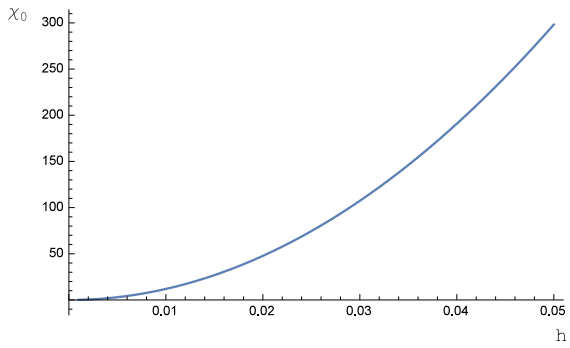

(a) h, half of the thickness of the plate is varied from 0.001 to 0.05, a quadratic dependence between h and χ_0 is observed.

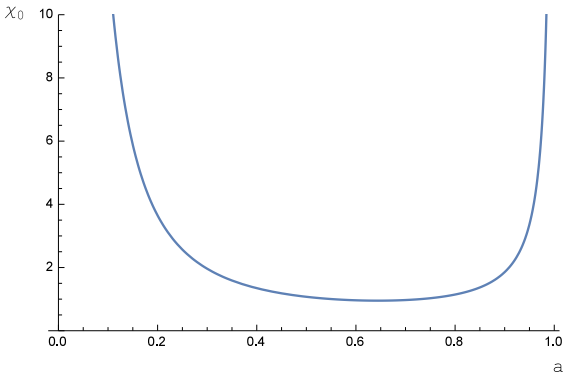

(b) a, the radius of the wetted inner circle is varied from 0.05 to 0.99. Two asymptotes, at $a = 0$ and $a = 1(= R)$ are observed, as we expect from physical considerations.

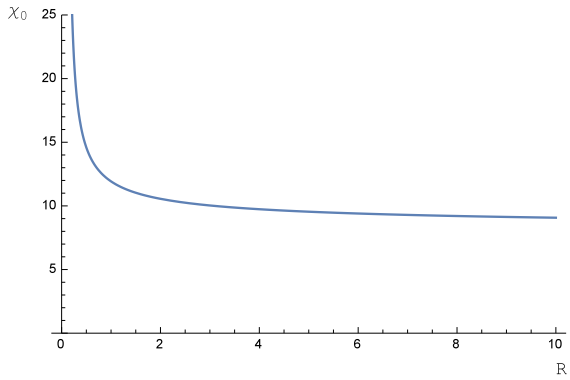

(c) R, the radius of the plate is varied between 0.2 and 10. An asymptote at $R = 0.1(= a)$ is observed. The buckling threshold χ_0 decreases as R grows and converges to a certain limit.

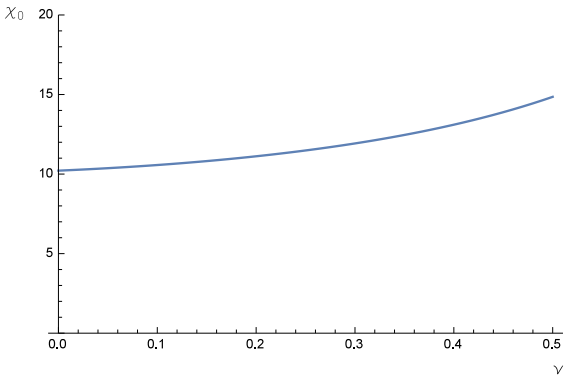

(d) ν, Poisson's ratio is varied between 0 and 0.5, the buckling threshold χ_0 changes only slightly.

Figure 6.7: The dependence of the buckling threshold χ_0, shown on the vertical axis, for four parameters.

6.1.2 Comparison of the simulation and the analysis

We will compare the results of the simulation to the analytical determination of the buckling threshold. We will explore the boundaries of which parameter values the simulation and the analytical method are capable of handling, staying in accordance with one another. Figure 6.8 shows the dependence on h for both methods. We see a good agreement for values of $h \leq 0.02$.

The discrepancy for larger values of h can be explained by the limited validity of the Von Kármán model: the radius to thickness ratio becomes smaller than 25, while we assumed that the thickness is negligible compared to the in-plane dimensions. Although most of the literature remains vague on the limits of the thickness in order for the model to remain valid, in [8] it is suggested that ratios above 10 should provide good results. Since the details of the numerical method used in the simulation are not publicly available, we do not know whether it compensates for the limitations of the von Kármán model for thicknesses at the edge of the desired range or not. Regardless, we should note that the simulation and analytical results agree only for small values of h; for these specific parameter values $h < 0.02$. Drawing a parallel to the case of an A4 paper sheet, with a width to thickness ratio of about $100 - 200$, this should not pose a problem.

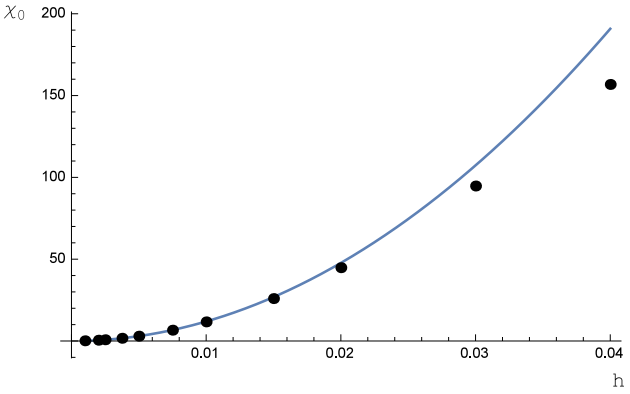

Figure 6.8: The buckling threshold is shown in dependence of half the thickness, h, resulting from the simulation (black dots) and the analysis (blue line). The remaining parameter values are given at the beginning of this chapter.

When the wetted part of the plate becomes either large or small, the buckling threshold χ_0 becomes high. Also it could be difficult to capture the behavior of the small region, the dry and the wetted part respectively, in the simulation. For small values of a extra attention is paid to this, since the boundary conditions to prevent rigid body movements are imposed at the center. The comparison between simulation and analysis for various values of a is shown in Figure 6.9.

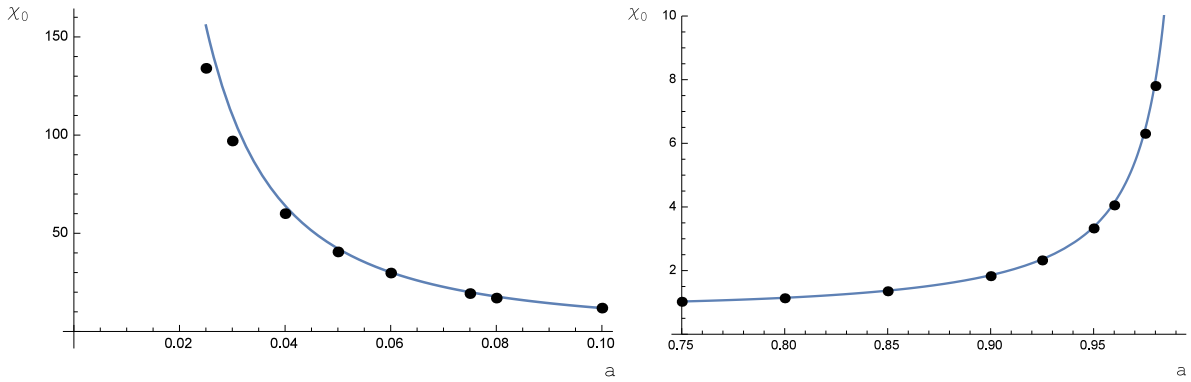

(a) The buckling threshold χ_0 is shown for low values of a, resulting from the simulation (black dots) and the analysis (blue line).

(b) The buckling threshold χ_0 is shown for high values of a, resulting from the simulation (black dots) and the analysis (blue line).

Figure 6.9: Comparison of the two methods for determining the buckling threshold χ_0 for both low values and high values of a. The remaining parameter values are given at the beginning of this chapter.

The simulation results agree with the analytical ones, except for low values of a. Considering these results

with regard to the paper sheet, caution should be taken when simulating a situation in which the wetted area is small compared to the sheet dimensions. Then again, in this instance, probably this reduces to a pre-buckling model in which the Kirchhoff model can be used, which simplifies matters.

The dependence of the buckling threshold on the radius of the plate R is shown in Figure 6.10. An excellent agreement is shown, even for small values of R down to twice the moistened part of the plate.

Now that we have explored the behavior of the buckling threshold near the limits of the admissible parameters values, we will consider the range of parameter values corresponding to wetting paper. The parameter values considered are:

- $\nu = 0.1,\ 0.4.$
- $R = 0.1\text{m},\ 1\text{m}.$
- $R/a = 2,\ 20.$
- $R/h = 500,\ 5000.$

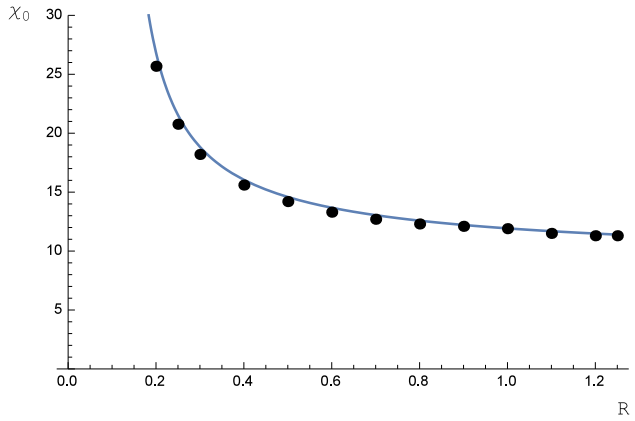

Figure 6.10: The buckling threshold χ_0 is shown in dependence of the radius of the plate, R, resulting from the simulation (black) and the analysis (blue). The remaining parameter values are given at the beginning of this chapter.

The material properties of the paper sheet in most imaginable paper wetting situations will be inside this range. We compare the simulation to the analysis for these 16 instances. The results are shown in Table 6.1. It should be noted here that the results for $R/h = 5000$ were hard to obtain, because the magnitude of the forces applied to obtain imperfections must be limited to a small interval. Nevertheless, the results from the simulation align well with the analytically obtained values of the buckling threshold. We conclude based on the results for this reference

ν	R	R/h	R/a	χ_0, Marc/Mentat	χ_0, Analysis
0.1	0.1	500	2	0.036	0.036
			20	1.5	1.5
		5000	2	0.0021	0.0021
			20	0.015	0.015
	1	500	2	0.036	0.036
			20	1.5	1.5
		5000	2	0.00036	0.00036
			20	0.016	0.015
0.4	0.1	500	2	0.048	0.048
			20	1.8	1.8
		5000	2	0.00048	0.00048
			20	0.019	0.018
	1	500	2	0.048	0.048
			20	1.9	1.8
		5000	2	0.00048	0.00048
			20	0.019	0.018

Table 6.1: The comparison between the buckling threshold χ_0 obtained from the simulation and from the analysis is made for various values of the relevant parameters in the range of the problem of a wetted paper sheet.

problem that the simulation and the analytical method agree well on describing the wetting of a paper sheet

up to the onset of buckling. However, this reference problem differs from the situation of interest on two essential features:

- The effect of orthotropy of the sheet is not taken into account.
- The reference problem contains no corners.

To compare the simulation and the analysis when these effects are included we will next consider the rectangular plate.

6.2 Rectangular plates

The results of the simulation and the analytical solution for the reference problem of the rectangular plate problem from Chapter 4 will be discussed here. We will consider four reference plates:

- Plate 1: square 1×1m isotropic plate with $E = 10^9$Pa, $h = 0.0005$m and $\nu = 0.3$ exposed to the moisture profile shown in Figure 6.11a.
- Plate 2: 1×1.5m isotropic plate with $E = 10^9$Pa, $h = 0.0005$m and $\nu = 0.3$ exposed to the moisture profile shown in Figure 6.11b.
- Plate 3: 1×1.5m orthotropic plate with 0.0005m, $E_x = 8 \cdot 10^9$Pa, $G_{xy} = E_y = 2 \cdot 10^9$Pa, $\nu_{xy} = 0.3$, $\beta_y = 5\beta_x$ exposed to the moisture profile shown in Figure 6.11b.
- Plate 4: 0.2×0.3m orthotropic plate with otherwise the same parameter values as plate 3 exposed to the moisture profile shown in Figure 6.11b.

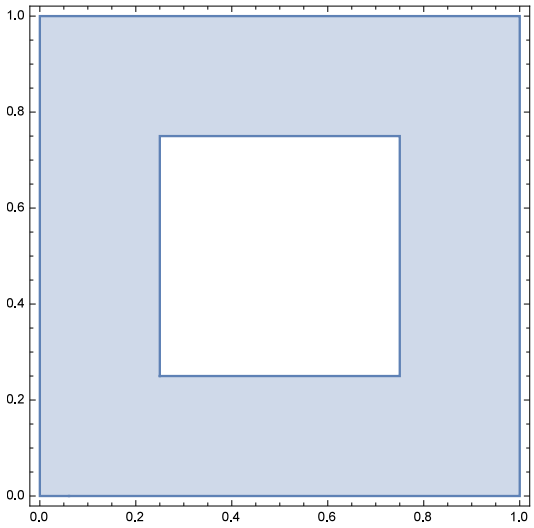

(a) The wetted region (in blue) of the plate 1. The moisture penetrates up to 1/4 in both directions

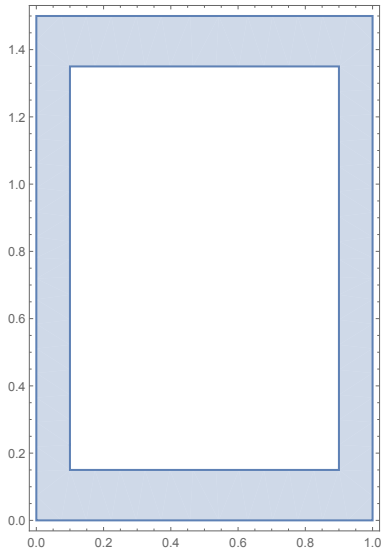

(b) The wetted region (in blue) of Plate 2,3 and (scaled) 4. The moisture penetrates up to $1/10^{\text{th}}$ of the plate.

Figure 6.11: The moisture distributions used for the reference problems.

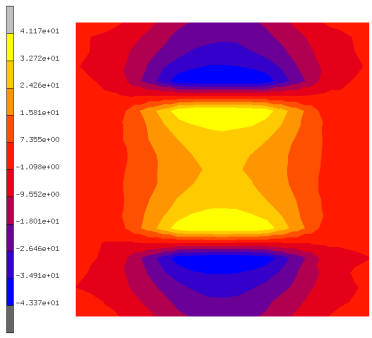

(a) Simulation results for σ_{xx}

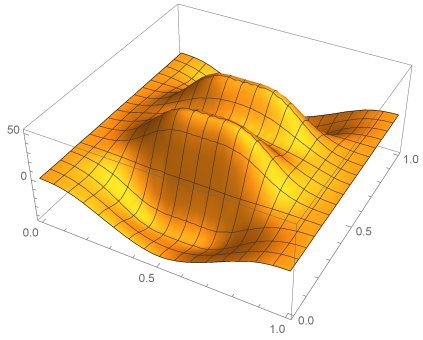

(b) Analytical results for σ_{xx}

Figure 6.12: Comparison of the stresses of plate 1 found using the simulation and the analysis, with $\beta\chi = 10^{-7}$.

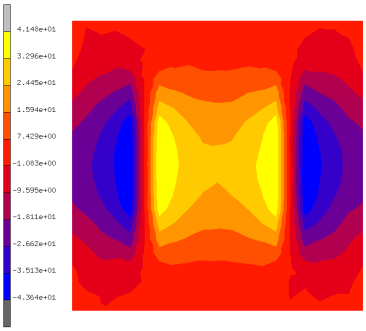

(a) Simulation results for σ_{yy}

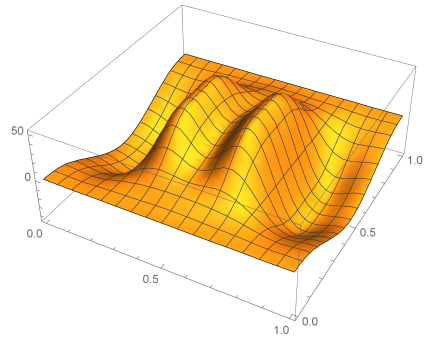

(b) Analytical results for σ_{yy}

Figure 6.13: Comparison of the stresses of plate 1 found using the simulation and the analysis, with $\beta\chi = 10^{-7}$.

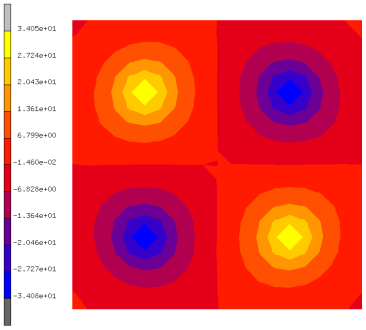

(a) Simulation results for σ_{xy}

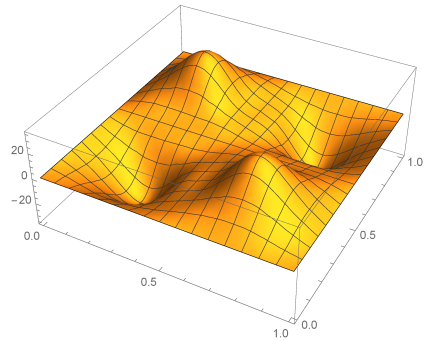

(b) Analytical results for σ_{xy}

Figure 6.14: Comparison of the stresses of plate 1 found using the simulation and the analysis, with $\beta\chi = 10^{-7}$.

The stress profiles of plate 1 obtained by means of the two methods are compared. As we can see in Figures 6.12, 6.13, 6.14, the stress profiles obtained by means of the analysis are very similar to the results of the simulation. This similarity has also been observer for the remaining three plates. Next we use the

implementation of the Rayleigh-Ritz method in Wolfram Mathematica [16] to approximate the buckling threshold for the plates, and compare the results to the values obtained in the simulation:

The calculations in Mathematica, are done by approximating the clamped beam functions (4.8) with a Fourier series for efficiency. We also make use of the symmetry in the plates chosen to reduce the calculations required for numerical integration. A slightly modified version of this file could be used to obtain results for non-symmetrical situations. As coordinate functions for the deflection we use a Fourier cosine series, or a polynomial with even powered terms, as discussed in Section 4.2. Both have been tried with various amounts of terms. It showed that adding terms beyond 10 does not substantially change the results. Keeping the number of terms limited to 10 results in the Mathematica file calculating the buckling threshold within a couple of minutes.

The Rayleigh-Ritz method is a good way to quickly obtain an estimate for the buckling threshold. Even a very crude estimation of the deflected shape will result in a decent approximation of the buckling threshold. However, precisely because of this, it is less suitable to find the post-buckling shape of the plate. We will content ourselves with the comparison of the buckling thresholds obtained from the analysis and the simulation. Table 6.2 shows this for the four plates.

Plate	$\beta_x\chi$, Rayleigh-Ritz	$\beta_x\chi$, Simulation
1	$8.1 \cdot 10^{-8}$	$7.5 \cdot 10^{-8}$
2	$6.2 \cdot 10^{-8}$	$5.6 \cdot 10^{-8}$
3	$2.8 \cdot 10^{-8}$	$2.6 \cdot 10^{-8}$
4	$7.0 \cdot 10^{-7}$	$6.4 \cdot 10^{-7}$

Table 6.2

As we can see the Rayleigh-Ritz method produces higher values than the simulation. This is to be expected, because with the simple coordinate functions it only gives a crude estimation of the buckling threshold and because it always overestimates the energy minimum. In all four cases, the buckling threshold obtained using the Rayleigh-Ritz method is about 10% higher than the value from the simulation. This leads us to the conclusion that the results from the simulation are consistent with the Rayleigh-Ritz analysis.

Chapter 7

Conclusions and recommendations

7.1 Summary

The goal of this thesis is to gain insight in the underlying physical process causing deformations of wetted sheets of paper. Particular emphasis has been put on behavior for stress levels up to and including the buckling threshold. Two approaches have been applied: theoretical analysis and simulation using FEM software.

The research topic is a largely unexplored area, since most articles in this direction assume clamped or simply supported boundary conditions. These boundary conditions were not suitable for the present work, since in the practical situation at Océ large deflections have been observed at the edges of the sheets. The freely moveable boundary conditions complicate matters.

A geometrically non-linear elasticity model based on Von Kármán large displacement theory was derived to describe the behavior of thin plates, and solution methods were applied two reference problems: an isotropic circular plate, wetted at the center, and a rectangular orthotropic plate moisturized at its edges.

The isotropic circular plate problem has been solved directly, which was possible under the assumption of axisymmetry. The solution, consisting of the stress distribution, the buckling threshold and the shape formed immediately after buckling, has been found in terms of Bessel functions. The influence of the relevant parameters has been described. Young's modulus E turned out to have no effect on the buckling threshold. This is explained by the fact that bending and stretching energy both depend linearly on this material property. Since it was also found that Poisson's ratio ν has little effect on the buckling threshold, the conclusion can be drawn it is largely geometrically determined. Three parameters determine the geometry: the radius R, the thickness $2h$ and the radius of the wet circle a. The radius to thickness ratio is especially important, since validity of the Von Kármán model depends on it. As for the case of paper, this probably poses no problem due to its thin nature. The buckling threshold has been found to depend quadratically on this ratio: the thicker the plate, the more stress it takes to buckle. The dependence of the buckling threshold on the ratio of the radii of the plate and the wet area respectively, R/a shows two asymptotes: for a completely dry and a completely wet plate no buckling will occur. Between these two asymptotes a convex relation has been found. The reference problem of the rectangular plate has been tackled using variational methods. The stress distribution has been found and an approximation of the buckling threshold is given.

Using the commercially available finite element software package Marc/Mentat the deformations have been simulated for the two reference problems. The setup and working of the simulation were explained as much as possible, given that the details of the inner workings of the simulation are not published in the user documents. The settings required to obtain a good result have been described. They lead to a robust simulation running within a couple of minutes. The FEM calculations make use of shell elements and are based on Von Kármán theory. In the simulations the moisture content of the wetted area is raised in steps to accurately determine the buckling threshold. To prevent rigid-body movement the center of the plate is fixed to prevent it from moving or rotating in any direction. To initiate out-of-plane deformations an

imperfection has been applied. For the circular plate a force in the thickness direction has been applied at the start of the simulation, whereas the initial z-coordinates of the rectangular plate have been varied prior to the simulation. Randomizing the z-coordinates of the circular plate would probably yield good results as well, this has not been tried because an imperfection force yielded good results.

The results from the analytical method and the simulations have been compared. In the pre-buckling moisture content range the components of displacement and stress show a good agreement, for both the circular and the rectangular plate. For the circular plate, the results from the two approaches for the buckling threshold and the post-buckling shape have shown to match well inside a range of parameter values where realistically paper sheets would fall into.

The pre-buckling stress of rectangular plates wetted at the edges has been determined through variational analysis and simulation. The results agree well. The buckling threshold obtained using the Rayleigh-Ritz method was consistently about 10% higher than the one obtained using Marc Mentat for the four plates under consideration.

Based on the results obtained with regard to the comparison between the simulation and the analysis, we draw the conclusion that the simulation captures the behavior of the wetted sheet well, up to and including the onset of buckling. Because of the confidence with which we can say that the simulation has been validated, we would advice to use this simulation to obtain results for more complicated situations.

7.2 Suggestions for further research

Due to time constraints, a parameter study has not been conducted for the reference problem of the rectangular plate as part of this thesis. It is recommended to verify the validity of the simulation for a range of parameter values, as has been done for the reference problem with the circular plate. Special attention should be paid to the effect of orthotropy, since this has not been considered yet. From the Von Kármán equations (2.84), (2.85),

$$\frac{E_x}{G_{xy}} - 2\nu_{xy}, \qquad \nu_{yx} + \frac{(1-\nu_{xy}\nu_{yx})G_{xy}}{E_x}, \qquad \frac{E_x}{E_y}, \tag{7.1}$$

arise as candidates for the parameters quantifying orthotropy. In Von Kármán theory there are four independent material constants in an orthotropic medium; E_x, E_y, G_{xy} and ν_{xy} (or ν_{yx}. After the scaling with E_x three remain, as in (7.1).

Also, the simulated behavior of the sheet near the corners should be looked at in detail and compared with the analytical results.

The results obtained in this thesis are theoretical and remain far from the real-life situation obtained at Océ. To come closer to reality, a couple of extensions need to be applied to the model. This can be done using the simulation which has now been validated for moisture content levels up to and including the buckling threshold. We give a list of suggestions:

- The simulation provides options to add a second body to serve as the foundation on which the sheet rests. This severely complicates matters however, since contact problems are notoriously difficult in finite element analysis. A logical step is then to add effects of gravity and friction to the simulation. Suggestions on how to add a frictionless elastic foundation to the Von Kármán formulation for analytical purposes can be found in [13], Chapter 4.

- It would be interesting to gain insight into the moisture-induced deformations of stacks of paper. Applying the theory mentioned in the preceding suggestion to model contact between sheets could prove helpful in this instance.

- The post-buckling shape for the rectangular plate obtained through simulation, a simple half-wave, differs from the wavy pattern observed in reality. This could have two causes:

  - The shape formed by the paper is a minimization of the potential energy at stress levels far beyond the onset of buckling, which causes it to be different from the one right after buckling. At moisture content levels not too far beyond the buckling threshold these modes can be determined by considering the other eigenvalues of (4.18).
  - Localized buckling occurs due to imperfections in the sheet, causing large deflections at multiple locations along the sheet edge. Much research has been conducted on plate buckling with initial imperfections when simply supported boundaries are assumed. See for example [13], where an initial imperfection has been added to various reference problems.

- A simple moisture distribution has been assumed throughout this thesis: a region of the paper which is uniformly wetted and a region which remains at its initial moisture content level. To obtain practical results, a more realistic moisture distribution obtained by means of a diffusion analysis should be applied. This does make the integral required to determine the stress distribution (4.15) more difficult to calculate.

- The relevant material properties, Young's moduli, shear modulus, Poisson's ratio, depend on the moisture content of the sheet [3], §7.5. An analysis of the extent to which this affects the moisture-induced deformations of paper in the conditions encountered at Océ is recommended. Marc/Mentat allows a user-defined linear temperature(moisture content)-dependence of the material properties to be included in the simulation.

- A typical sheet of paper consists of 10 layers in the thickness direction[3]. Using composite plate theory, this can be represented in the Von Kármán model [13] to obtain better results. This theory is also available in Marc/Mentat by defining a multi-layered shell element. Introducing multiple layers can be useful to better represent the shear stresses in the sheet and allow for moisture content differences in the thickness direction. Since the theory allows for differences in material properties amongst the respective layers, this can be used to account for coatings, layers at the upper and lower side of the paper with properties vastly different from the remainder of the sheet. Coatings are present at virtually any type of paper used for printing purposes.

- As discussed in Section 1.2, paper is a very heterogeneous material due to its manufacturing process. Local variations of height, fibre alignment, density, and Young's and shear moduli are expected to heavily influence the resulting deformations. Specifically, during the simulations conducted to write this thesis, a big influence of height differences on the out-of-plane displacements has been observed when the randomized z-coordinates of the initial position were varied too much. Much research has been done on stochastic mechanics. However, an extensive research into the effects of local changes would be complicated and time-consuming due to the large number of parameters involved.

- In this research the effects due to repeated wetting and drying, hysteresis effects, have been neglected. Many of the properties of paper depend on its moisture history [3]. Since during the manufacturing process of paper many large changes in moisture content are required, permanent deformations occur, which affect the deformations the paper exhibits when it is used for printing. A micro-scale model of these hysteresis effects would help our understanding of the resulting material properties and imperfections.

This page is intentionally left in its initial, undeformed, configuration.

Bibliography

[1] Océ Varioprint i300 product brochure, available online here

[2] G. Goldmann, L. Michel, The world of printers, technologies of Océ printing systems. Chapter 6: Paper, a living material. Océ, 2001.

[3] K. Niskanen, Mechanics of paper products. De Gruyter, 2012.

[4] M.A.L.J. Fransen, Transient moisture exchange between paper and environment, master thesis, Eindhoven university of technology, 2010.

[5] I.S. Sokolnikoff, Mathematical theory of elasticity. McGraw-Hill, 1946.

[6] A.A.F. van de Ven, Continuum mechanics, Eindhoven university of technology, 2009.

[7] S. Timoshenko, S Woinowsky-Krieger, Theory of plates and shells. McGraw-Hill, 1959

[8] E. Ventsel, T. Krauthammer, Thin plates and shells, theory analysis and applications. Marcel Dekker Inc., 2001.

[9] S.G. Lekhnitskiy, Anisotropic plates. Translation by USA foreign technology division, 1957.

[10] M. Abramowitz, I.A. Stegun, Handbook of mathematical functions, 1972.

[11] K. Washizu, Variational methods in elasticity and plasticity, Pergamom press, 1982.

[12] D.J. Mead, Vibration and buckling of flat free-free plates under non-uniform in-plane thermal stress, Journal of sound and vibration 260, 2003

[13] H.S. Shen, A two-step perturbation method in nonlinear analysis of beams, plates and shells, Wiley, 2013

[14] Marc Mentat version 2014.0.0 Beta, MSC software.

[15] MATLAB version R2013b, Mathworks.

[16] Wolfram Mathematica version 10.0

[17] MSC. Marc volume A: theory and user information.

[18] MSC. Marc volume B: element library.